Journal of Materials Chemistry C

PAPER

View Article Online
View Journal | View Issue

Cite this: J. Mater. Chem. C, 2016, 4, 7061

Star-shaped D–π–A oligothiophenes with a tris(2-methoxyphenyl)amine core and alkyldicyanovinyl groups: synthesis and physical and photovoltaic properties†

Yuriy N. Luponosov,‡*[a] Jie Min,‡*[b] Alexander N. Solodukhin,[a] Artem V. Bakirov,[ac] Petr V. Dmitryakov,[ac] Maxim A. Shcherbina,[ad] Svetlana M. Peregudova,[ae] Georgiy V. Cherkaev,[a] Sergei N. Chvalun,[ac] Christoph J. Brabec[bf] and Sergei A. Ponomarenko[ag]

Received 14th April 2016,
Accepted 18th June 2016

DOI: 10.1039/c6tc01530a

www.rsc.org/MaterialsC

Synthesis of a series of star-shaped oligomers having a novel electron donating tris(2-methoxyphenyl)-amine (m-TPA) core, which is linked through a bithiophene or terthiophene π-bridge with electron-deficient alkyldicyanovinyl (alkyl-DCV) groups, is described. A comprehensive study of the oligomers revealed significant dependence of their physical properties, including absorption, molecular frontier energy levels, crystal packing, and melting and glass transition temperatures, upon the chemical structure. A comparison of their photophysical properties to the nearest analog having the common dicyanovinyl (DCV) groups demonstrated a number of benefits to use alkyl-DCV units for the design of donor–acceptor small molecules: higher solubility, increased electrochemical stability, better photovoltaic performance, and possibility to control the relative physical and photovoltaic properties by a simple adjustment of alkyl and π-bridge lengths. Modification of the well-known triphenylamine (TPA) core in the star-shaped oligomers by methoxy groups increases not only solubility, but also crystallinity of the oligomers, whereas their photovoltaic performance stays on a similar level as their analogs with a TPA core. The study demonstrates that these design strategies represent interesting and simple tools for the effective modulation of properties of star-shaped molecules.

1. Introduction

Solar cells based on organic semiconductors are developing as a promising cost-effective alternative to silicon-based solar cells due to their easy fabrication by solution processing, lightweight, and compatibility with flexible substrates.[1–3] Despite the fact that conjugated polymers are dominating the field of bulk heterojunction (BHJ) organic solar cells (OSCs),[4] small molecules are receiving increasing attention due to their well-defined molecular structures, ease of functionalization, amenability to standard organic purification and characterization methods, and reduced batch-to-batch variability. Recently, there has been significant progress in the development of small molecules for use in BHJ OSCs.[5–7] The dynamic development of solution-processed small molecule OSCs has recently led to high power conversion efficiencies (PCEs) of over 10%.[8,9] Despite that the development of cheap and stable photoactive materials as well as novel design strategies for small molecules is still key to boost their potential for commercial applications.

Oligothiophenes and their derivatives with well-defined structures possess extensive π-electron delocalization along the molecular backbone and are well known as good hole-transporting materials.[10] Despite their excellent semiconducting properties, they do not absorb strongly in the red and

[a] Enikolopov Institute of Synthetic Polymeric Materials of the Russian Academy of Sciences, Profsoyuznaya st. 70, Moscow 117393, Russia. E-mail: luponosov@ispm.ru
[b] Institute of Materials for Electronics and Energy Technology (I-MEET), Friedrich-Alexander-University Erlangen-Nuremberg, Martensstraße 7, 91058 Erlangen, Germany. E-mail: Min.Jie@fau.de
[c] National Research Centre "Kurchatov Institute", 1, Akademika Kurchatova pl., Moscow, 123182, Russia
[d] Moscow Institute of Physics and Technology, 4 Institutsky line, Dolgoprudny, Moscow region, 141700 Russian Federation
[e] Nesmeyanov Institute of Organoelement Compounds, Russian Academy of Sciences, Vavilova St. 28, Moscow, 119991, Russia
[f] Bavarian Center for Applied Energy Research (ZAE Bayern), Haberstraße 2a, 91058 z, Germany
[g] Chemistry Department, Moscow State University, Leninskie Gory 1-3, Moscow 119991, Russia

† Electronic supplementary information (ESI) available: ^{1}H and ^{13}C NMR spectra, molecular modeling, X-ray diffraction data, and photovoltaic data. See DOI: 10.1039/c6tc01530a

‡ These authors contributed equally to this work.

near-infrared parts of the spectrum where most solar photons are concentrated. Inclusion of electron-withdrawing units to the oligothiophene backbone can extend their absorption spectrum toward longer wavelengths by an intramolecular charge transfer (ICT) and thus lead to a better match with the solar spectrum. For this purpose, the dicyanovinyl (DCV) unit is one of the widely used acceptor groups due to its strong electron-accepting character.[11,12] A main drawback of the DCV group is the presence of an active vinyl hydrogen,[13,14] which decreases the stability of the materials. The replacement of the active hydrogen by an alkyl group was found to be an efficient tool not only to increase the electrochemical stability of donor–acceptor small molecules,[15,16] but also to control their solubility and a number of important solid-state physical properties by simple adjustment of the alkyl chain length in the DCV substituent.[17,18]

To fine-tune the energy levels in small molecules, some additional electron-donating blocks such as dithienosilole,[19–22] benzodithiophene,[23,24] and dithienopyrrole,[25] and *etc.*, are often used. For the design of star-shaped molecules, a triphenylamine (TPA) core is one of the widely used electron-donating blocks due to its low cost, high electrochemical stability and hole transporting ability.[12,26,27] Moreover, the propeller-like structure of TPA prevents strong π–π interactions between neighboring groups, so that the vast majority of TPA derivatives are amorphous and highly soluble materials. In order to optimize the photophysical properties of TPA-based star-shaped oligomers, a few attempts to modify the TPA block were done, which were based mainly on its planarization strategy.[28–31] Nevertheless, an increase in the performance of organic field-effect transistors (OFETs),[28] organic light-emitting diodes (OLEDs)[29] and OSCs[28,30] as compared to the devices based on non-modified analogs, revealed great potential of TPA modification for moderately and effectively tuning the properties of star-shaped molecules.

Meanwhile, alkoxy substituents at the phenyl rings of TPA have been successfully used in the design of asymmetrical D–A molecules for organic and hybrid organic solar cells.[32,33] Alkoxy substituents at the TPA core can increase the solubility, change intra- and intermolecular interactions as well as energy levels of the molecules, and thus influence the solid-state properties of pristine oligomers and their blends. However, the first example of a D–A star-shaped molecule with alkoxy groups at TPA, namely with the tris(2-methoxyphenyl)amine (m-TPA) core, has been reported recently.[34]

In this work we report on the synthesis and a comprehensive study of a series of four D–π–A oligomers having the tris-(2-methoxyphenyl)amine (m-TPA) core as a donor, either alkyl-DCV or DCV as acceptor units, and either bi- or terthiophene as π-bridges (Scheme 1). A comparison of properties of these four molecules with those of their full analogs with a TPA core[15–17,35] reveals the benefits and drawbacks of this chemical design strategy. Furthermore, variation of the π-bridge and the alkyl chain length as well as the type of substituent at the DCV group allows elucidating the structure–property relationships in this series of star-shaped molecules systematically.

2. Results and discussion

2.1 Synthesis and chemical characterization

Synthesis of star-shaped oligomers with m-TPA and alkyl-DCV groups, N(Ph-OMe-2T-DCV)$_3$, N(Ph-OMe-2T-DCV-Me)$_3$,[35] N(Ph-OMe-3T-DCV-Et)$_3$, and N(Ph-OMe-3T-DCV-Hex)$_3$, was carried out using our recently developed approach for their analogs with the TPA core.[15,16] The synthetic routes outlined in Scheme 2 include several key reaction stages: preparation of the initial aldehyde or ketones (Schemes 2a and b), synthesis of an organoboron derivative of bi- or terthiophene precursors (Scheme 2c), and preparation of star-shaped precursors with protective groups followed by the deprotection reaction and substitution of carbonyl functions by DCV groups (Scheme 2d). However, in this work, several important optimizations of the initial steps were elaborated to simplify the synthesis. First, preparation of ketones, **1b–c**, was carried out by Friedel–Crafts acylation of 2,2′-bithiophene in the presence of tin chloride in 80–86% yields. This optimization allows using less expensive precursors and reagents as compared to manganese-catalyzed acylation of the magnesium derivative of 5-bromo-2,2′-bithiophene.[15,16] Nevertheless, it should be noted that the Friedel–Crafts acylation reaction was found to proceed with low reaction yields in the case of terthiophenes. Therefore, the extension of the oligothiophene length (preparation of **4b–c**) was carried out *via* Suzuki cross coupling between organoboron derivatives of dioxane-protected bithiophene ketones (**3b–c**) and 2-bromothiophene in 71–74% yields. Second, protection of carbonyl functions of the ketones was found to be more convenient with 5,5-dimethyl-1,3-dioxane groups as compared to previously used 1,3-dioxolane ones, due to higher stability and better isolated yields of the protected compounds.

Note that for the synthesis of the model star-shaped molecule with DCV groups, N(Ph-OMe-2T-DCV)$_3$, we have used for the first time a similar strategy as employed for the molecules with alkyl-DCV groups, whereas their common preparation is based on Vilsmeier–Haack formylation of star-shaped oligothiophenes followed by Knöevenagel condensation.[12,16] The main difference in the synthetic route for N(Ph-OMe-2T-DCV)$_3$, as compared to the molecules with alkyl-DCV groups, is preparation of the aldehyde precursor (**1a**) instead of the ketone one, which was done by lithiation of commercially available 2,2′-bithiophene followed by its reaction with dimethylformamide (DMF) in 94% yield. In addition, there were also variations in the rates of protection, deprotection and Knöevenagel reactions due to different activities of ketones and aldehydes (see the Experimental section for details).

As a result, all target star-shaped oligomers under discussion were prepared in good reaction yields, while their chemical structures and high purity were proved by ^{1}H-, and ^{13}C-NMR spectroscopy, elemental analysis, and mass-spectroscopy (see ESI,† Fig. S1–S35). The low reaction yield of N(Ph-OMe-3T-DCV-Et)$_3$ can be explained by losses incurred during purification by column chromatography, because of its insufficient solubility in dichloromethane, which was used as an eluent. All these oligomers obtanied demonstrate reasonable solubility in common

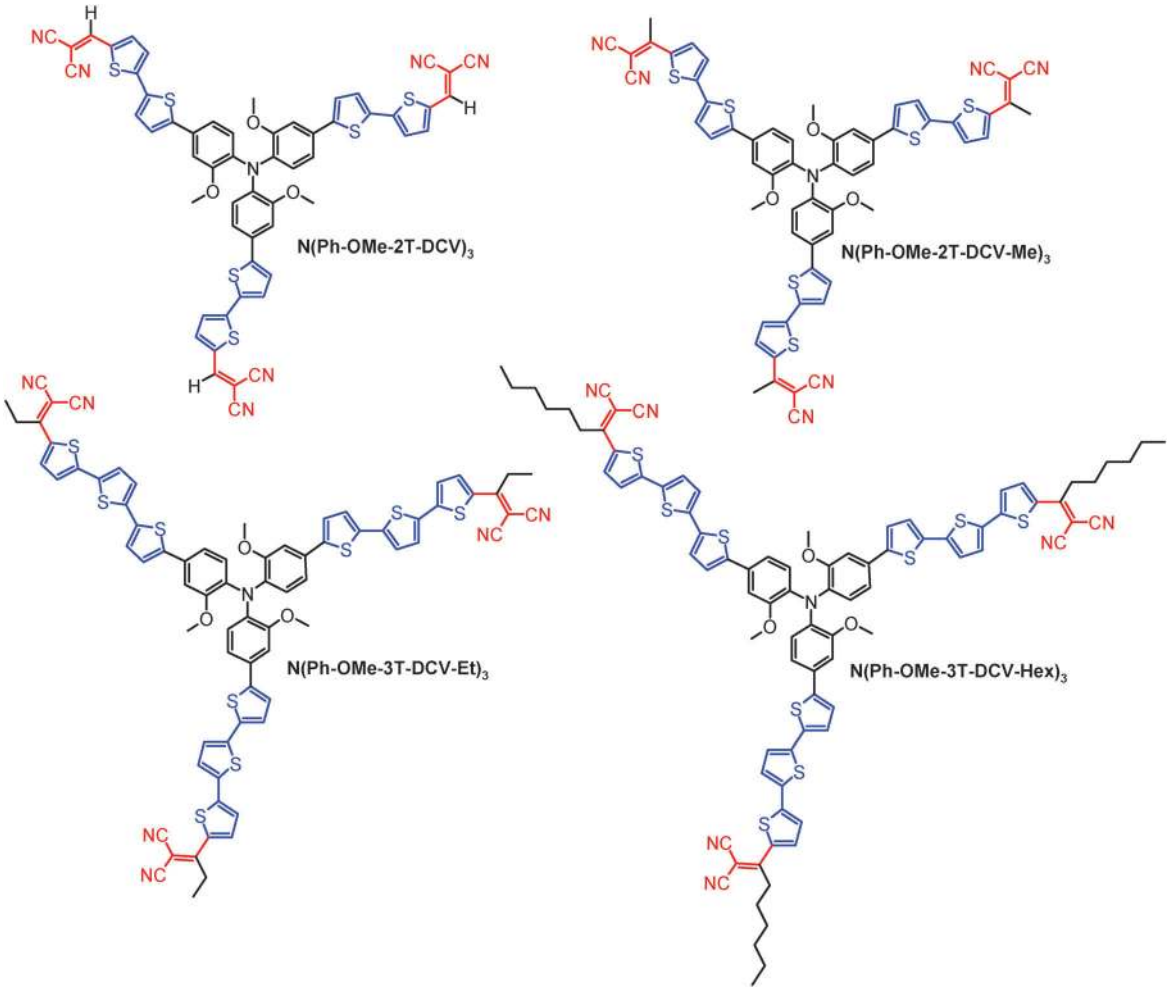

Scheme 1 Chemical structures of the star-shaped D–π–A oligomers investigated.

organic solvents such as THF, chloroform, and 1,2-dichlorobenzene (ODCB).

2.2 Solubility and thermal properties

The exact values of solubility for all star-shaped oligomers prepared were measured in ODCB at room temperature (Table 1). One can see that the solubility in this series of molecules depends significantly on the chemical structure and tends to decrease with elongation of the π-bridge length and increase with elongation of the alkyl chain length. The lowest solubility was found for the model molecule without terminal alkyl groups, N(Ph-OMe-2T-DCV)$_3$, and for N(Ph-OMe-3T-DCV-Et)$_3$ having the longest 3T arms and short ethyl groups. A comparison of the solubility values for the series of m-TPA-based molecules to those obtained for their full analogs with the TPA core revealed that the usage of the former core can increase the solubility by *ca.* 2–5 times (Table 1).

Thermal properties of the oligomers synthesized were investigated by thermogravimetric analysis (TGA) and differential scanning calorimetry (DSC). One can see that all these oligomers possess very high stability both in air and under an inert atmosphere (Fig. 1). Decomposition temperatures (T_d), corresponding to 5% weight loss, were found to be above 380 °C in air and under the inert atmosphere, as exhibited in Table 1. The residual weights vary from 50–75% upon heating up to 700 °C in nitrogen. A comparison of the weight loss at very high temperatures indicates that it is caused mostly by decomposition of the aliphatic groups. The influence of the terminal hydrogen in the DCV unit on the thermal stability of the oligomers cannot be evaluated by this technique, since the weight loss due to hydrogen elimination is around 0.2%, which is close to the experimental error.

DSC analysis (Fig. 2a and Table 2) reveals that all these oligomers as received are crystalline materials with relatively high values of melting temperature (T_m) and melting enthalpy (ΔH_m). However, the crystal structure was not restored after the first melting and subsequent cooling to room temperature. One can observe a glass transition in the second heating scans only (Fig. 2b), where a glass transition temperature (T_g) lies in the range of 74–147 °C. This peculiarity was used to simplify the dissolution of these compounds, since materials in the amorphous state dissolve much better as compared to the crystalline one. A comparison of T_m and ΔH_m values for the compounds studied allows concluding that elongation of the oligothiophene

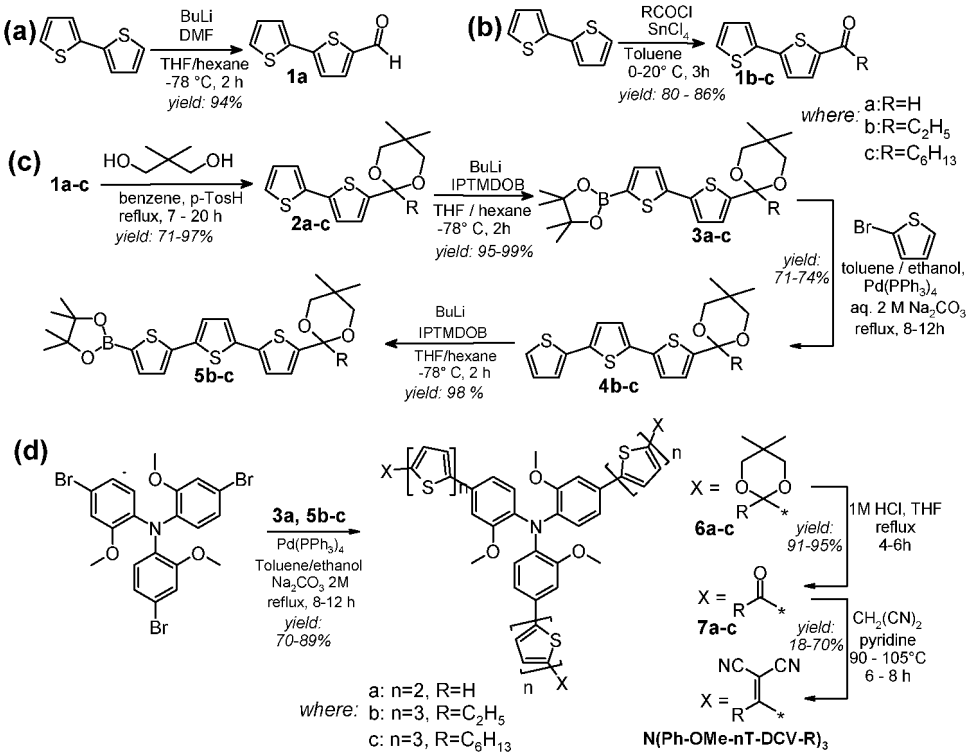

Scheme 2 Synthesis of N(Ph-OMe-2T-DCV)$_3$, N(Ph-OMe-3T-DCV-Et)$_3$, and N(Ph-OMe-3T-DCV-Hex)$_3$.

Table 1 Solubility and thermal properties of the star-shaped oligomers

		First heating		Second heating		TGA (air)	TGA (N_2)
Compounds	Solubility[a], mg mL^{-1}	T_m, °C	ΔH_m, J g^{-1}	T_g, °C	dC_p, J (g K)$^{-1}$	T_d, °C	T_d, °C
N(Ph-OMe-2T-DCV)$_3$	9	200	32	147	0.33	403	408
N(Ph-OMe-2T-DCV-Me)$_3$	14	248	54	130	0.23	415	402
N(Ph-OMe-3T-DCV-Et)$_3$	8	243	50	119	0.27	403	391
N(Ph-OMe-3T-DCV-Hex)$_3$	20	173	30	76	0.33	386	400
N(Ph-2T-DCV)$_3$[b]	2	276	28	145	0.17	405	405
N(Ph-2T-DCV-Me)$_3$[b]	3	270	82	136	0.26	416	416
N(Ph-3T-DCV-Hex)$_3$[b]	12	—	—	75	0.29	388	388

[a] Measured in ODCB. [b] Data from ref. 16; dC_p – heat capacity change at the glass transition; T_d corresponds to 5% weight loss.

π-bridge or shortening of the alkyl chains leads to improved ordering in the bulk.

It is interesting to compare phase behavior of the molecules with m-TPA core to their full analogs having the TPA core (see Table 1).[15–16,34] N(Ph-3T-DCV-Hex)$_3$, being the full analog of N(Ph-OMe-3T-DCV-Hex)$_3$ but with the TPA core, is characterized by a hexagonal columnar mesophase.[34] Meanwhile, N(Ph-2T-DCV)$_3$ and N(Ph-2T-DCV-Me)$_3$ can also be crystalline as received similar to their analogs with m-TPA core. Melting temperature and enthalpy in the pair of N(Ph-2T-DCV-Me)$_3$ and N(Ph-OMe-2T-DCV-Me)$_3$ are rather similar, while the melting temperature of N(Ph-2T-DCV)$_3$ is substantially higher than that of N(Ph-OMe-2T-DCV)$_3$, albeit their melting enthalpies being also close to each other.

2.3 X-Ray diffraction data

X-ray studies of as-received samples of the compounds with the m-TPA core revealed that all of them are highly crystalline materials with substantially different crystal lattices (Fig. 3). However, the small-angle region of diffractograms is dominated by a strong reflection corresponding to the periodicity of ~30 Å. Moreover, its fourth order reflection is also one of the strongest in the wide-angle region for all the compounds investigated. As the position of the mentioned reflection does not depend on the arm length of the specific star-shaped molecule, one can conclude that this periodicity is due to the stacking of the molecules one above the other. Molecular modelling of the compounds with m-TPA core revealed that such discotic motifs form pairs in which methoxy groups of both partners are oriented outwards, the distance between the molecules being 5.8 Å (see the discussion and Fig. S38 and S39 in the ESI†). The same pairs are also the most specific feature of the crystal structure of the m-TPA compound.[36] A comparison of the experimental macroscopic densities with the calculated crystalline ones allows suggesting that molecular pairs form the

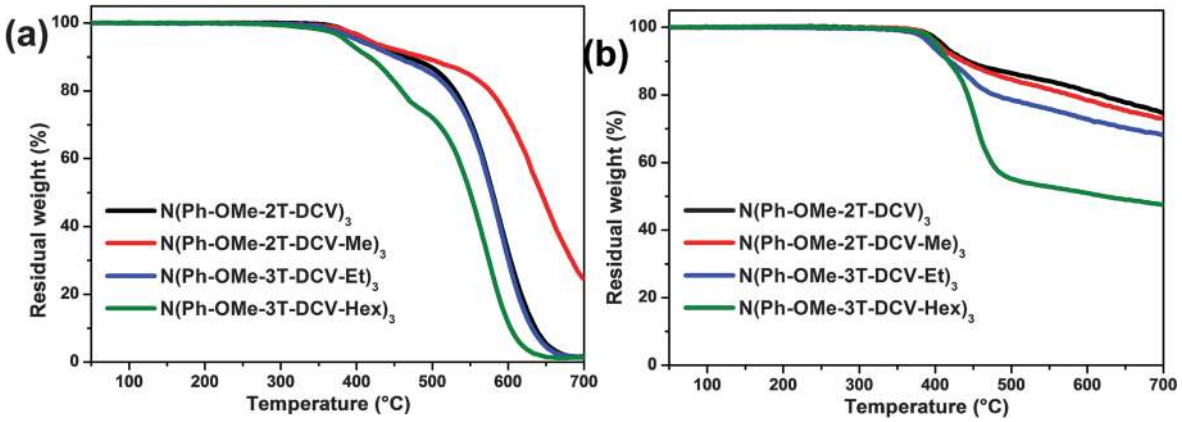

Fig. 1 TGA curves of star-shaped D–π–A oligomers (a) in air and (b) under nitrogen.

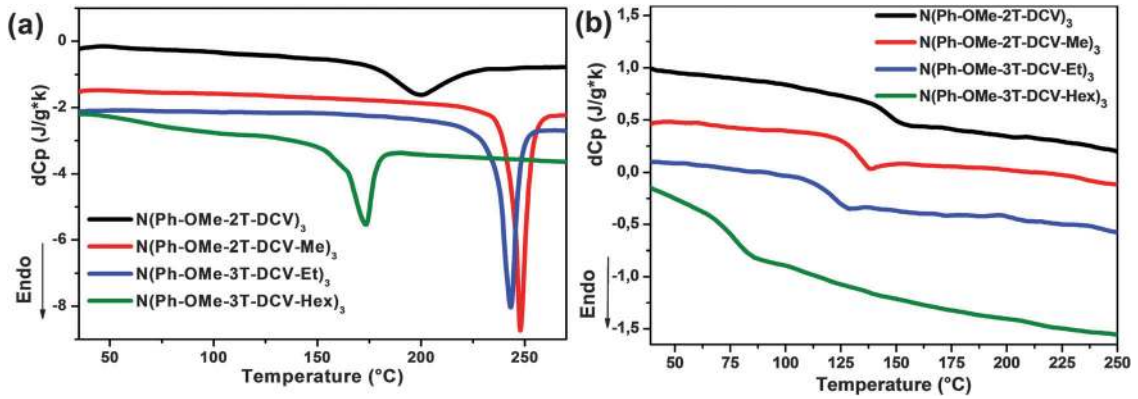

Fig. 2 DSC first (a) and second (b) heating scans of star-shaped D–π–A oligomers with m-TPA core.

Table 2 Calculated crystal lattice parameters and experimentally measured densities for compounds with m-TPA cores

Compounds	Type	a, Å	b, Å	c, Å	ρ_{calc}, g cm^{-3}	ρ_{exp}, g cm^{-3}	L_{arm}, Å
N(Ph-OMe-2T-DCV)$_3$	Orthorhombic	25.3	20.9	30.7	1.296	1.322	14.9
N(Ph-OMe-2T-DCV-Me)$_3$	Orthorhombic	20.7	18.8	33.3	1.693	1.303	16.1
N(Ph-OMe-3T-DCV-Et)$_3$	Orthorhombic	32.9	17.7	28.4	1.557	1.319	22.1
N(Ph-OMe-3T-DCV-Hex)$_3$	Orthorhombic	33.9	31.2	27.7	1.411	1.227	26.5

columns with an inner 3_1 or 3_2 helical ordering which is rather common for the compounds with the molecules possessing a rotary axis of symmetry of third order.

Excluding reflections corresponding to the periodicity along the columns, one can obtain parameters of the column ordering in the lateral direction. Here two main criteria of choice correctness were used – first, a comparison of calculated and experimental densities and the arm length. We should though notify in advance that the macroscopic density was measured using the bulk samples after their melting and subsequent cooling, *i.e.* amorphous ones (Table 2). Thus, we allowed the calculated crystal density to be 10–15% higher than the experimental one. Second, all the reflections observed should have been indexed (see Tables S1–S4 in ESI†).

Fig. 4 shows the 001 cleavage planes of calculated crystal lattices. One should remember that every molecule on such a cleavage represents the whole 3_1 helical column. However, every hand of the molecule has a face-to-edge π–π stacking with the molecule in the neighboring column, thus providing a helical pathway for charge carriers. The length of the star's arm varies from 14.9 to 26.5 Å. All the lattices, with the exception of that formed by N(Ph-OMe-3T-DCV-Hex)$_3$, contain two columns with different types of rotations (one in the middle and four quarters in the corners). Thus, one can observe the layers of the columns of particular orientation alternating with the layers of the columns of an opposite one. The crystal lattice formed by the compound N(Ph-OMe-3T-DCV-Hex)$_3$ contains three columns (two in the middle and four quarters in the corners) and the corresponding three different types of column layers. This fact could be due to a substantial length of hands of a particular star-shaped molecule, so that the packing of two different layers still leaves too much free space.

Summing up the structural information concerning the star-shaped compounds with and without methoxy groups in

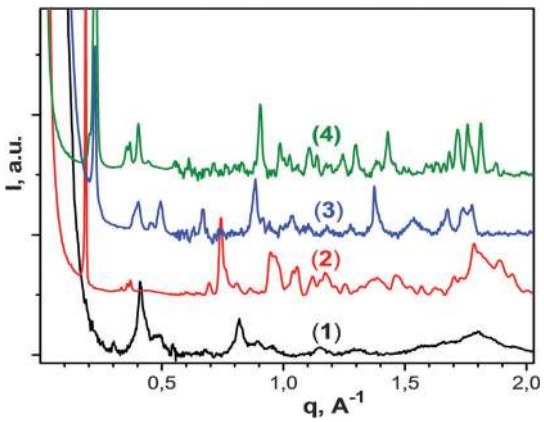

Fig. 3 X-Ray scattering patterns for N(Ph-OMe-2T-DCV)$_3$ (**1**), N(Ph-OMe-2T-DCV-Me)$_3$ (**2**), N(Ph-OMe-3T-DCV-Et)$_3$ (**3**) and N(Ph-OMe-3T-DCV-Hex)$_3$ (**4**).

their TPA cores, one can conclude that methoxy groups play a definitive role in the formation of pair aggregates inside the supramolecular columns, which are not observed in TPA-based analogs. Such aggregates are responsible for substantially higher ordering and the formation of crystal structures in the materials with methoxy groups in the TPA cores. In comparison, formation of ordered structures in the compounds without methoxy groups in TPA cores is considerably hindered.

2.4. Optical and electrochemical properties

The UV-vis absorption spectra of the star-shaped oligomers in dilute ODCB solutions and thin films are shown in Fig. 5. Samples used for the measurements of film absorption spectra were prepared by doctor-blading from ODCB solutions. The corresponding optical data are summarized in Table 3. In ODCB, all compounds demonstrate similar spectra: the weak UV absorption peak (370–412 nm) as generally accepted corresponds to the π–π* transition and the intensive visible peak (520–540 nm) is attributed to the ICT transition between the m-TPA-oligothiophene donor and the alkyl-DCV or DCV acceptor units.[12] However, it has been shown that in fact both electronic excitations have a mixed character and the intensity of the high-energy absorption feature is a direct measure of the degree of conformational disorder in the star-shaped molecule.[37] Indeed, with an increase of the π-conjugated bridge length from 2T to 3T the shorter wavelength region peaks are red-shifted from 375 nm to 412 nm, which is attributed to the stronger localized π–π* transition for the 3T π-bridge. Interestingly, the expected red-shifts of low energy bands for molecules with 3T π-bridges were not observed, since the extension of the conjugation cannot compensate the decrease in ICT between the core and the terminal DCV units caused by a longer distance between them and intramolecular distortions in the 3T chain. A comparison with the absorption bands of the star-shaped molecules based on alkyl-DCV units as acceptor groups in films, the low energy absorption band is red-shifted by 16 nm for N(Ph-OMe-2T-DCV)$_3$ due to somewhat stronger electron-withdrawing ability of DCV groups.[15] In thin films, the optical spectra of all these star-shaped molecules become broader and maxima of their absorption peaks (λ_{max}) shift to a long-wave region as compared to those observed in solutions (Fig. 5b).

The electrochemical properties of the four star-shaped molecules and their highest occupied molecular orbital (HOMO) and lowest unoccupied molecular orbital (LUMO) energy levels

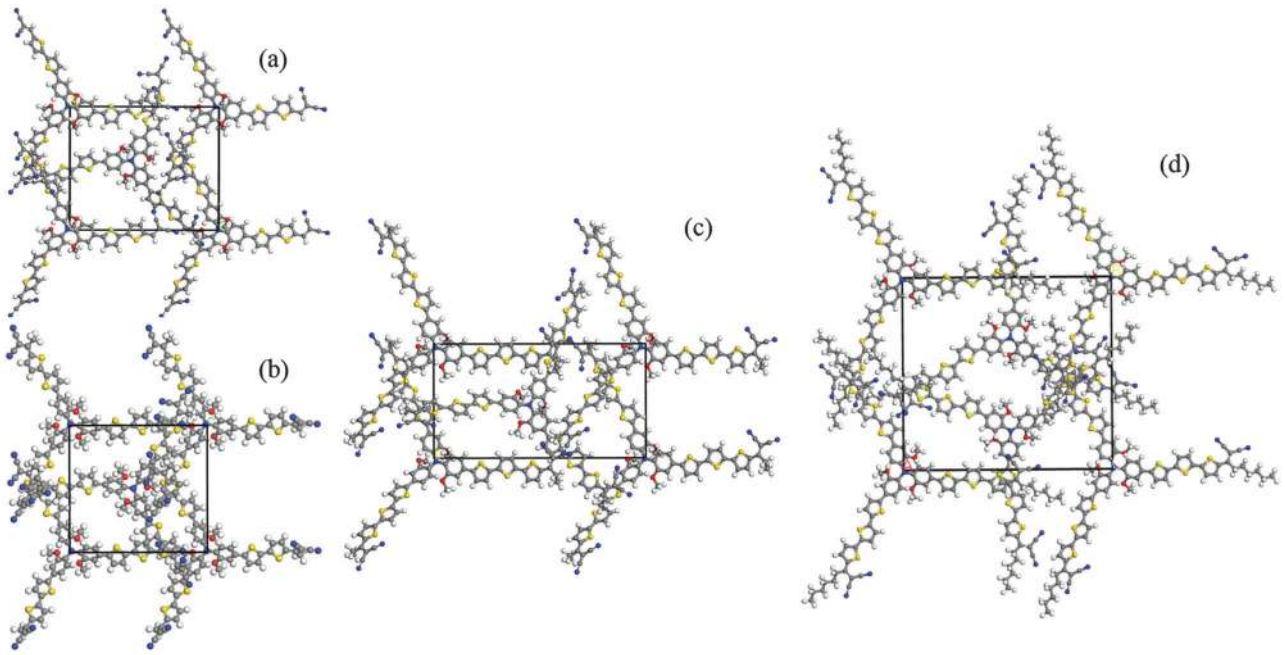

Fig. 4 Packing of the molecules in crystal lattices calculated based on X-ray scattering patterns for N(Ph-OMe-2T-DCV)$_3$ (a), N(Ph-OMe-2T-DCV-Me)$_3$ (b), N(Ph-OMe-3T-DCV-Et)$_3$ (c) and N(Ph-OMe-3T-DCV-Hex)$_3$ (d).

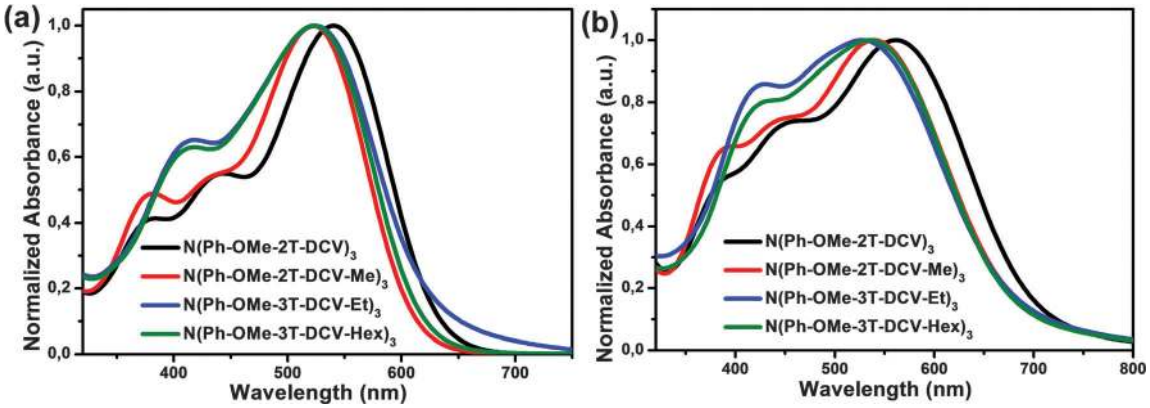

Fig. 5 UV-vis absorption spectra of m-TPA-based oligomers in (a) dilute ODCB solutions and in (b) films cast from ODCB.

Table 3 Optical and electrochemical properties of the investigated m-TPA-based oligomers

	UV-vis absorption				Cyclic voltammetry		
	Solution[a]	Film[b]			Oxidation	Reduction	
Compounds	λ_{max} (nm)	λ_{max} (nm)	λ_{onset} (nm)	$E_g^{opt\,c}$ (eV)	$\varphi_{ox}{}^{d}$/HOMO (V)/(eV)	$\varphi_{red}{}^{d}$/LUMO (V)/(eV)	E_g^{EC} (eV)
N(Ph-OMe-2T-DCV)$_3$	377/540	456/562	707	1.75	0.80/−5.20	−0.94/−3.46	1.74
N(Ph-OMe-2T-DCV-Me)$_3$	376/524	452/542	688	1.80	0.80/−5.20	−1.02/−3.38	1.82
N(Ph-OMe-3T-DCV-Et)$_3$	412/524	428/531	688	1.80	0.74/−5.14	−1.03/−3.37	1.77
N(Ph-OMe-3T-DCV-Hex)$_3$	412/524	432/535	688	1.80	0.74/−5.14	−1.03/−3.37	1.77

[a] Measured in ODCB solution. [b] Cast from ODCB solution. [c] Bandgap estimated from the onset wavelength (λ_{edge}) of the optical absorption: $E_g^{opt} = 1240/\lambda_{edge}$. [d] Standard formal reduction (φ_{red}) and oxidation (φ_{ox}) potentials *vs.* SCE obtained for films of the oligomers.

were examined by cyclic voltammetry (CV) (see Table 3 and Fig. 6). From these data, it is clearly seen that all molecules demonstrate similar oxidation behavior, which appears as two consecutive and fully reversible waves. A decreased value of the first standard formal oxidation potential (φ_{ox}) values for N(Ph-OMe-3T-DCV-Et)$_3$ and N(Ph-OMe-3T-DCV-Hex)$_3$, as compared to 2T-contaning analogs, revealed that elongation of the π-bridge length facilitates the oxidation process. However, influence of the π-bridge length on the first standard reduction potential (φ_{red}) was not observed, because in this process the reduction of DCV groups occurs firstly. Therefore, somewhat a different φ_{red} value (−0.94 V *vs.* −1.03 V relative to SCE) was observed for N(Ph-OMe-2T-DCV)$_3$ having common DCV groups, which indicates its hindered reduction. Another important difference between the molecules having either DCV or alkyl-DCV groups is irreversibility of the reduction process for the former due to the presence of active vinyl hydrogens in their structure. In Fig. 6, one can see that the reduction of all compounds with alkyl-DCV groups proceeds with the first reversible and the second irreversible waves, whereas reduction of N(Ph-OMe-2T-DCV)$_3$ goes with the first irreversible wave only. These observations indicate the lower stability of anion radicals for oligomers having active hydrogen at DCV groups, whereas replacement of the vinyl hydrogens with alkyl groups stabilizes the anion radicals and increases their electrochemical stability.

The HOMO and LUMO energy levels were calculated using first standard formal oxidation and reduction potentials according

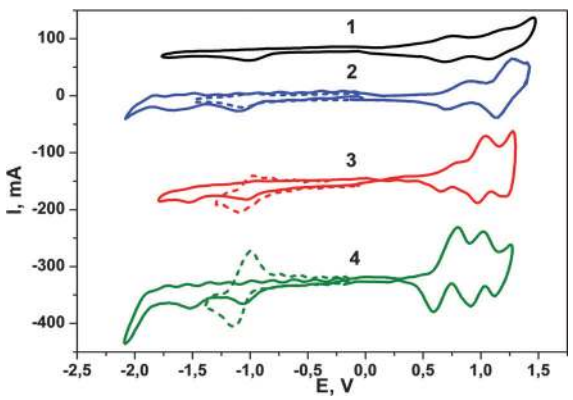

Fig. 6 Cyclic voltammograms of N(Ph-OMe-2T-DCV)$_3$ (**1**), N(Ph-OMe-2T-DCV-Me)$_3$ (**2**), N(Ph-OMe-3T-DCV-Et)$_3$ (**3**) and N(Ph-OMe-3T-DCV-Hex)$_3$ (**4**). Insets (dashed curves) correspond to the cyclic voltammogram of the first wave.

to the following equation: LUMO = $e(\varphi_{red} + 4.40)$ (eV) and HOMO = $-e(\varphi_{ox} + 4.40)$ (eV).[38] For N(Ph-OMe-3T-DCV-Et)$_3$ and N(Ph-OMe-3T-DCV-Hex)$_3$ the LUMO was found to be −3.37 eV, which is similar to N(Ph-OMe-2T-DCV-Me)$_3$, whereas the HOMO was found to be −5.14 eV, which shows a bit lowered bandgap of 1.77 eV as compared to 1.82 eV for their 2T-containing analogue. The lowest electrochemical bandgap value (1.74 eV) was observed for N(Ph-OMe-2T-DCV)$_3$, which is in good agreement with its optical bandgap (see Table 1). Compared to their analogues with TPA core,[16] this series of star-shaped molecules shows somewhat

higher HOMO levels due to the presence of additional electron donating methoxy substitutes in the m-TPA core.

2.5 Charge transport

Since the intended application of the star-shaped molecules under study is as a donor component in mixtures with the acceptor component $PC_{70}BM$ in BHJ OSCs, a space charge limited current (SCLC) method was used to map out the hole- and electron-only mobilities of the oligomers/$PC_{70}BM$ blended films. The *J–V* characteristics of both hole-only and electron-only diodes can excellently fit to the Mott–Gurney model (Fig. 7). We calibrated the hole (μ_h) and electron (μ_e) mobilities by fitting the current–voltage curves over six diodes. The related average values of hole- and electron-only mobilities of the blended films are given in Table 4. All devices based on the star-shaped molecules with alkyl-DCV groups demonstrated slightly higher hole-only mobilities, but lower electron-only mobilities as compared to their analogue with DCV groups, N(Ph-OMe-2T-DCV)$_3$. A comparison of the devices based on N(Ph-OMe-2T-DCV-Me)$_3$ and N(Ph-OMe-3T-DCV-Et)$_3$ showed that elongation of the oligomer π-bridge length from 2T to 3T does not influence significantly the mobility in blends. While the increase of the alkyl chain length from ethyl to hexyl in N(Ph-OMe-3T-DCV-Et)$_3$/N(Ph-OMe-3T-DCV-Hex)$_3$ systems leads to an obvious decrease of both the hole and electron mobilities. This observation, on the one hand, can be explained by the poorer blend morphology of the N(Ph-OMe-3T-DCV-Hex)$_3$: $PC_{70}BM$ system as shown below. On the other hand, elongation of the alkyl chain results in the weakening of the intra- and intermolecular interactions in the solid state, which is in agreement with our previous results as well as the thermal properties of pristine oligomers.[34] A comparison of the hole-only mobility of N(Ph-OMe-2T-DCV-Me)$_3$ and N(Ph-OMe-3T-DCV-Hex)$_3$ to the values obtained for their full analogs with the TPA core[34] revealed a bit higher mobility for the blends based on the molecules with m-TPA core. These results regarding charge transport properties of blends will further influence the device performance as discussed below.

2.6. Photovoltaic properties of BHJ devices

To study the effects of the donor core, acceptor group, oligothiophene π-bridge length and alkyl chain length on the photovoltaic properties, BHJ OSCs with a configuration of ITO/PEDOT:PSS/oligomer:$PC_{70}BM$ (wt%)/ZnO(25 nm)/Al(100 nm) were fabricated, and the detailed device fabrication process is described in the Experimental section. The corresponding parameters of devices with the best blending ratios are shown in Fig. S40 (ESI†), while optimized performances of these devices were achieved with the weight ratio of 1 : 2 or 1 : 2.5 without any treatments, as shown in Fig. 8a and summarized in Table 5.

As expected, OSCs based on N(Ph-OMe-2T-DCV)$_3$ and N(Ph-OMe-2T-DCV-Me)$_3$ show relatively high V_{oc} up to 0.9 V, due to their low-lying HOMO energy levels. With an increase of the π-conjugated oligothiophene bridge length, OSCs based on N(Ph-OMe-3T-DCV-Et)$_3$ and N(Ph-OMe-3T-DCV-Hex)$_3$ showed lower V_{oc} values of 0.82 V and 0.86 V, respectively. These results are attributed to their HOMO level variations (Fig. 8c) and also consistent with our previous results.[16,35] In addition, the slightly higher V_{oc} values (see Fig. 8c) for N(Ph-OMe-2T-DCV-Me)$_3$ and N(Ph-OMe-3T-DCV-Hex)$_3$ as compared to N(Ph-OMe-2T-DCV)$_3$ and N(Ph-OMe-3T-DCV-Et)$_3$ may be explained by the presence of longer terminal alkyl groups for the former, leading to a weakening of the intermolecular interactions between the donor and the acceptor moieties.[17,39] Among these four systems, OSCs based on N(Ph-OMe-2T-DCV-Me)$_3$ exhibit the highest J_{sc} values (see Fig. 8d), resulting from the high and balanced charge transport properties. The N(Ph-OMe-3T-DCV-Hex)$_3$ system in contrast exhibits the poorest J_{sc} value, probably due to the longest alkyls at DCV, suppressing the intramolecular and intermolecular interactions.[17] The corresponding J_{sc} values are consistent with the external quantum efficiency (EQE) measurements (see Fig. 8b). In addition, these devices exhibited similar FF values of *ca.* 50% (see Table 5). Finally, the PCEs of these devices are 3.73% for N(Ph-OMe-2T-DCV)$_3$, 4.38% for N(Ph-OMe-2T-DCV-Me)$_3$, 3.55% for N(Ph-OMe-3T-DCV-Et)$_3$ and 3.18% for N(Ph-OMe-3T-DCV)$_3$, respectively. In general, the PCEs of OSCs based on molecules with m-TPA core and alkyl-DCV groups are slightly lower but comparable with those obtained for their analogs with TPA

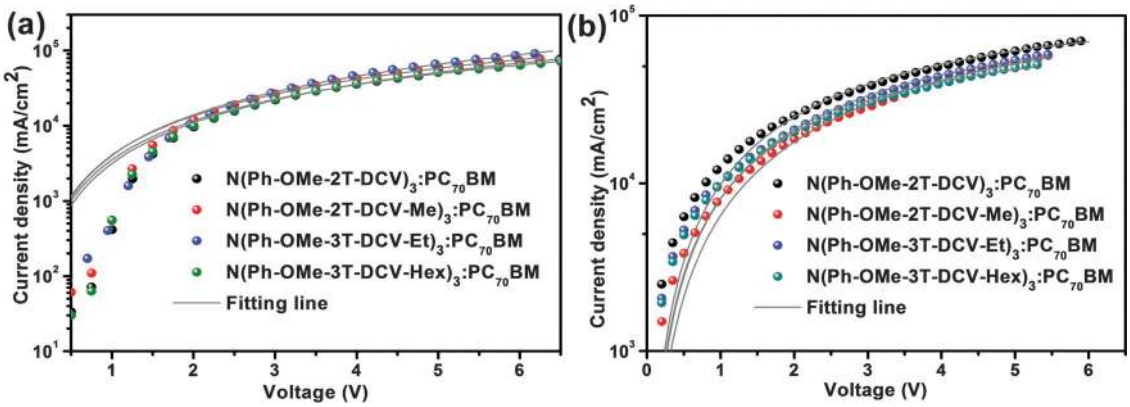

Fig. 7 The dark *J–V* characteristics of devices based on the m-TPA core oligomers including hole-only (a) and electron-only (b) devices. The solid lines represent the best fitting using the SCLC modified Mott–Gurney model.

Table 4 Hole- and electron-only mobilities determined from the SCLC measurements

Semiconductor layers	Thickness (nm)	μ_h[a] [$cm^2 V^{-1} s^{-1}$]	Thickness (nm)	μ_e[a] [$cm^2 V^{-1} s^{-1}$]	μ_e/μ_h
N(Ph-OMe-2T-DCV)$_3$: $PC_{70}BM$ (1 : 2.5)	81	4.58×10^{-4}	70	1.27×10^{-3}	2.77
N(Ph-OMe-2T-DCV-Me)$_3$: $PC_{70}BM$ (1 : 2)	86	6.07×10^{-4}	75	8.15×10^{-4}	1.34
N(Ph-OMe-3T-DCV-Et)$_3$: $PC_{70}BM$ (1 : 2)	78	5.87×10^{-4}	75	9.91×10^{-4}	1.69
N(Ph-OMe-3T-DCV-Hex)$_3$: $PC_{70}BM$ (1 : 2.5)	85	4.86×10^{-4}	74	6.73×10^{-4}	1.38

[a] The reported mobility data are average values of the blended films over six devices.

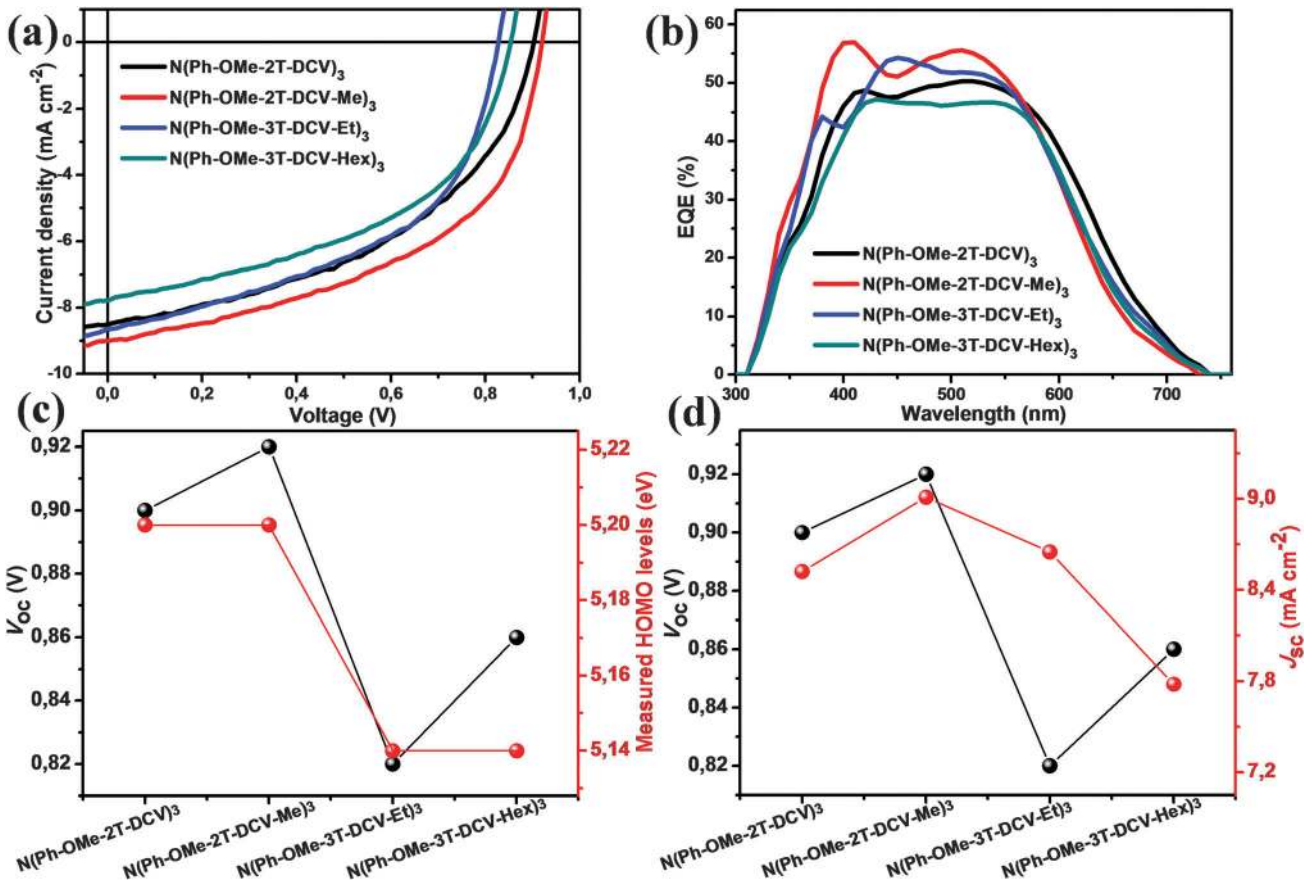

Fig. 8 Current density–voltage (I–V) curves (a) and EQE spectra (b) of solar cells based on N(Ph-OMe-2T-DCV)$_3$: $PC_{70}BM$ (1 : 2.5, wt%), N(Ph-OMe-2T-DCV-Me)$_3$: $PC_{70}BM$ (1 : 2, wt%), N(Ph-OMe-3T-DCV-Et)$_3$: $PC_{70}BM$ (1 : 2, wt%), and N(Ph-OMe-3T-DCV-Hex)$_3$: $PC_{70}BM$(1 : 2.5, wt%), respectively, under the illumination of AM 1.5G light, 100 mW cm^{-2}; the correlation between: (c) V_{oc} and experimental HOMO values of m-TPA based molecules and (d) V_{oc} and J_{sc} values of the OSCs based on these four systems.

Table 5 Photovoltaic properties of oligomer : $PC_{70}BM$ OSCs, under the illumination of AM 1.5 light, 100 mW cm^{-2}

Donor	D : A [wt%]	V_{oc} [V]	J_{sc} [mA cm^{-2}]	FF [%]	PCE[a] [%]
N(Ph-OMe-2T-DCV)$_3$	1 : 2.5	0.90	8.52	48.6	3.73(3.62)
N(Ph-OMe-2T-DCV-Me)$_3$	1 : 2	0.92	9.01	52.8	4.38(4.18)
N(Ph-OMe-3T-DCV-Et)$_3$	1 : 2	0.82	8.65	50.0	3.55(3.44)
N(Ph-OMe-3T-DCV-Hex)$_3$	1 : 2.5	0.86	7.78	47.6	3.18(3.02)

[a] The average values of PCEs calculated from over six devices.

core.[16,35] However, an obvious improvement of the photovoltaic performance from 2.31% for the N(Ph-2T-DCV)$_3$ system to 3.73% for the N(Ph-OMe-2T-DCV)$_3$ system was found, which is attributed to better molecular solubility and blend morphology of the latter. In addition, compared to the photovoltaic performance of the molecules with bithiophene as π-bridges, further extending of π-bridges to terthiophene did not lead to any improvement of the device performance. Nonetheless, the results of N(Ph-OMe-3T-DCV-Et)$_3$ and N(Ph-OMe-3T-DCV-Hex)$_3$ in devices demonstrated that the longer alkyl terminal chains resulted in worse photovoltaic parameters due to the poor charge transport and worse blend morphology, which is in good agreement with the previous research on TPA-based star-shaped molecules.[17]

2.7 Film morphology

Absorption spectra and the electronic structure of the components as well as their charge transport properties in blends are

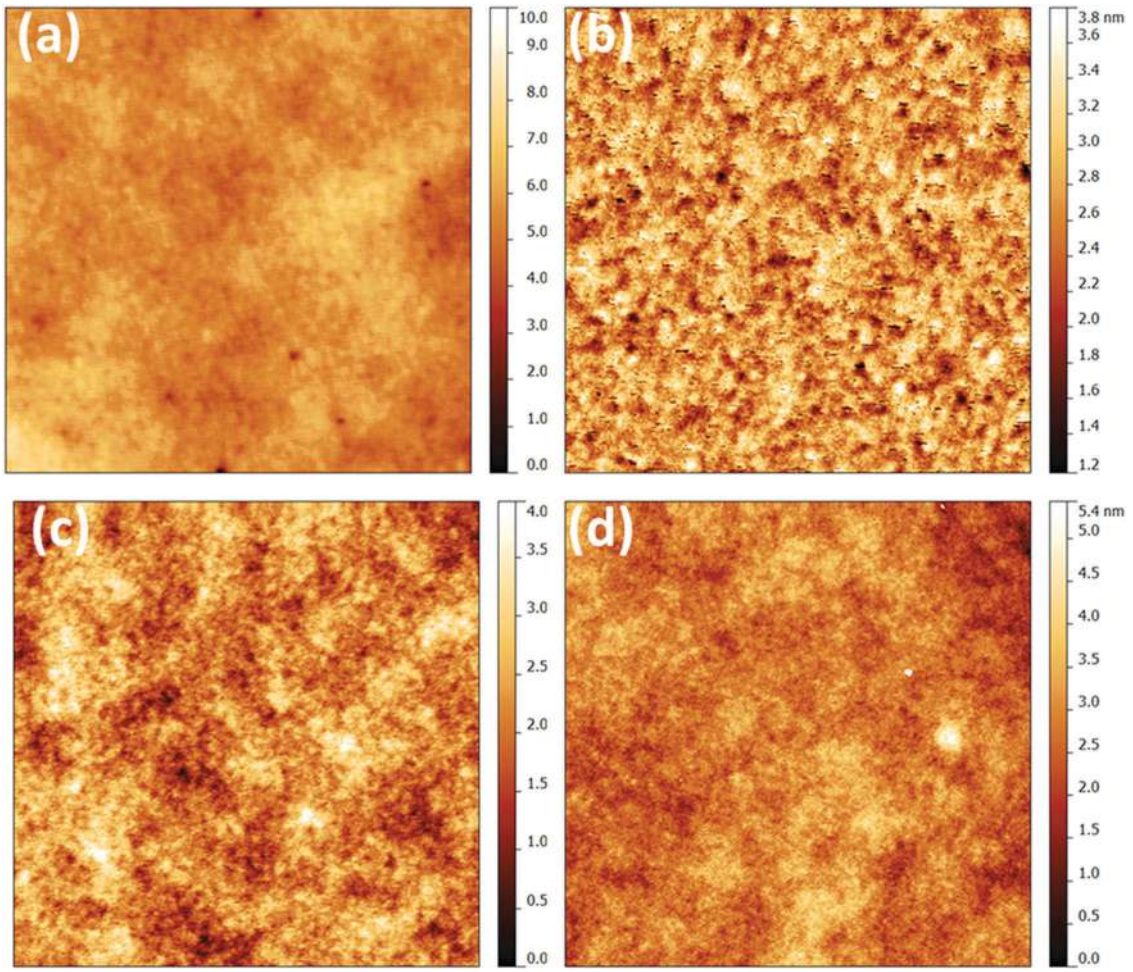

Fig. 9 Tapping mode AFM surface scans (5 × 5 μm^2) of blended films N(Ph-OMe-2T-DCV)$_3$: $PC_{70}BM$ (1 : 2.5 wt%) (a), N(Ph-OMe-2T-DCV-Me)$_3$: $PC_{70}BM$ (1 : 2 wt%) (b), N(Ph-OMe-3T-DCV-Et)$_3$: $PC_{70}BM$ (1 : 2 wt%) (c), and N(Ph-OMe-3T-DCV-Hex)$_3$: $PC_{70}BM$ (1 : 2.5 wt%) (d).

obviously important for device operation, but the role of film morphology cannot be ignored.[20] The topographic AFM images of the blended films determined for the optimized OSCs are given in Fig. 9.

All the blended films are rather smooth with an average surface roughness (RMS) of 0.61 nm, 0.35 nm, 0.46 nm and 0.54 nm for N(Ph-OMe-2T-DCV)$_3$: $PC_{70}BM$, N(Ph-OMe-2T-DCV-Me)$_3$: $PC_{70}BM$, N(Ph-OMe-3T-DCV-Et)$_3$: $PC_{70}BM$, and N(Ph-OMe-3T-DCV-Hex)$_3$: $PC_{70}BM$ films, respectively. However, in all cases, the blended film morphologies were slightly different. It is evident from AFM studies that the variations in the molecular size, the π-bridge and the alkyl length can cause changes in the microstructure of the blended films. Among these four blended films, the N(Ph-OMe-2T-DCV-Me)$_3$: $PC_{70}BM$ system exhibited the smallest RMS value. In addition, the most pronounced nanoscale-aggregation of the donor and acceptor phases was also found for the best performing N(Ph-OMe-2T-DCV-Me)$_3$: $PC_{70}BM$ system, indicating that these nanoscale domains are beneficial to the exciton charge separation and charge transportation and in turn enhance the device performance. Thus, a judicious choice of the core, oligothiophene π-bridge and alkyl chain length in star-shaped molecules is of crucial importance for fine-tuning the structure–morphology–property relationships.

3. Conclusions

In summary, we synthesized a series of star-shaped oligomers with a D–π–A structure and demonstrated the first comprehensive attempt to study the structure–property relationships depending on different substituents at donor and acceptor units as well as the length of either an oligothiophene π-bridge or terminal alkyl chain length. All these oligomers with a novel m-TPA core exhibit good solution processability and high thermal and thermooxidation stability. Various properties, such as solubility in organic solvents, phase behavior, crystal packing, HOMO/LUMO levels, charge-transport ability in blends, morphological characteristics and photovoltaic performance, can be fine-tuned simply by changing the π-bridge and the alkyl terminal chain length. On the one hand, the main benefits of usage of the alkyl-DCV acceptor groups to design star-shaped molecules are confirmed significantly by their higher solubility, electrochemical stability and photovoltaic performance as compared to normal DCV units.

On the other hand, the introduction of an m-TPA core, as compared to TPA, not only leads to higher solubility, but also possesses the possibility to obtain molecules in a crystalline state without significantly changing other photophysical and photovoltaic properties. Bearing the widespread usage of TPA-derivatives, we envisage that tris(2-methoxyphenyl)amine can find their own niche as a donor unit to design highly crystalline but still soluble semiconducting small molecules for organic and hybrid electronics.

4. Experimental section

4.1. Characterization

^{1}H NMR spectra were recorded on a ''Bruker WP-250 SY'' spectrometer, working at a frequency of 250.13 MHz and utilising the $CDCl_3$ signal (7.25 ppm) as the internal standard. ^{13}C NMR spectra were recorded using a ''Bruker Avance II 300'' spectrometer at 75 MHz. In the case of ^{1}H NMR spectroscopy, the compounds to be analysed were taken in the form of 1% solutions in $CDCl_3$. In the case of ^{13}C NMR spectroscopy, the compounds to be analysed were taken in the form of 5% solutions in $CDCl_3$. The spectra were then processed on the computer using ACD Labs software.

Mass-spectra (MALDI) were registered on an Autoflex II Bruker (resolution FWHM 18000), equipped with a nitrogen laser (working wavelength 337 nm) and a time-of-flight mass-detector working in the reflection mode. The acceleration voltage was 20 kV. Samples were applied to a polished stainless steel substrate. The spectrum was recorded in the positive ion mode. The resulting spectrum was the sum of 300 spectra obtained at different points of the sample. 2,5-Dihydroxybenzoic acid (DHB) (Acros, 99%) and α-cyano-4-hydroxycinnamic acid (HCCA) (Acros, 99%) were used as matrices.

Elemental analysis of C, H and N elements was carried out using a CHN automatic analyzer CE 1106 (Italy). The settling titration using $BaCl_2$ was applied to analyze sulphur. The experimental error for elemental analysis is 0.30–0.50%. The Knöevenagel condensation was carried out using a microwave ''Discovery'', (CEM Corporation, USA), using a standard method with the open vessel option, 50 watts.

Thermogravimetric analysis was carried out in dynamic mode in a 30–900 °C interval using a Mettler Toledo TG50 system equipped with an M3 microbalance. The heating/cooling rate was chosen to be 10 °C min^{-1}. Every compound was studied twice: in air and in a nitrogen flow of 200 mL min^{-1}. DSC scans were obtained using a Mettler Toledo DSC30 system with 20 °C min^{-1} heating/cooling rate in the temperature range of +20–250 °C for all compounds. A nitrogen flow of 50 mL min^{-1} was used.

Cyclic voltammetry measurements were carried out using solid compact layers of the oligomers, which in turn were made by electrostatically rubbing the materials onto a glassy carbon electrode. Measurements were made in CH_3CN : *o*-$C_6H_4Cl_2$ = 1 : 4 solution using 0.1 M Bu_4NPF_6 as a supporting electrolyte and using an IPC-Pro M potentiostat. The scan rate was 200 mV s^{-1}. The glassy carbon electrode was used as a working electrode. Potentials were measured relative to a saturated calomel electrode (SCE).

Absorption profiles were recorded using a Perkin Elmer Lambda-35 absorption spectrometer from 350 to 1100. AFM measurements were performed using a Nanosurf Easy Scan 2 in contact mode.

The structures of hole-only and electron-only devices were as follows: glass/ITO/PEDOT:PSS/semiconductor layer/MoO_3 (15 nm)/Ag (100 nm) and glass/ITO/ZnO/semiconductor layer/Ca (15 nm)/Ag (100 nm).

Small-angle diffraction patterns of high resolution were recorded using SAXS- and WAXS camera S3-Micropix, manufactured by Hecus (CuKα, λ = 1.542 Å). Two detectors were used: two-dimensional Pilatus 100K and linear gas position sensitive detector PSD 50M. For shaping the X-ray beam the Fox 3D vacuum optics were used, the slits in the Kratky collimator were set to 0.1 and 0.2 mm correspondingly. The angular scale was between 0.003 Å^{-1} and 1.9 Å^{-1}. The exposure varied from 600 to 5000 s while the Joule heater hot stages allowed heating the samples up to 300 °C.

The wide scattering angles were recorded at the Protein crystallography station at Kurchatov Synchrotron using a 2D detector MarCCD165 at a wavelength of 1.0402 Å (d$E/E = 2E^{-3}$). Station optics include a bending magnet with 1.7 T (E_c = 7.1 keV), a two-crystal monochromator with a focusing mirror resulting in a 2 × 1 mm^2 beam with a 10^{11}–10^{12} photons per mm^2 flux.

All devices were fabricated in the normal architecture. Photovoltaic devices were made by doctor-blading on indium tin oxide (ITO)-covered glass substrates (from Osram). These substrates were cleaned in toluene, water, acetone, and isopropyl alcohol. After drying, the substrates were bladed with 40 nm PEDOT:PSS (Heraeus Deutschland, PEDOT PH-4083). Photovoltaic layers, consisting of four different small molecules, were dissolved in ODCB with $PC_{70}BM$ as an acceptor with various weight ratios, and bladed on top of the PEDOT:PSS layer. The thicknesses of these blends are *ca.* 80–90 nm. After that, a ZnO layer (25 nm) was doctor-bladed on top of the active layer. Finally, an aluminum top electrode of 100 nm thickness was evaporated. The typical active area of the investigated devices was 10.4 mm^2. The current–voltage characteristics of the solar cells were measured under AM 1.5G irradiation on an OrielSol 1A solar simulator (100 mW cm^{-2}). The EQE was detected using a Cary 500 scan UV-Vis-NIR spectrophotometer under monochromatic illumination, which was calibrated with a mono-crystalline silicon diode. Absorption profiles were recorded using a Perkin Elmer Lambda-35 absorption spectrometer from 350 to 1100.

4.2 Materials

Tetrakis(triphenylphosphine)palladium(0)Pd(PPh_3)$_4$, 2,2′-bithiophene, *n*-butyl lithium (1.6 M solution in hexane), isopropoxy-4,4,5,5-tetramethyl-1,3,2-dioxaborolane (IPTMDOB), *p*-toluene sulfonic acid (*p*-TosH), heptanoyl chloride, acetyl chloride, DMF, 2,2-dimethylpropane-1,3-diol, and 2-bromothiophene malononitrile were obtained from Sigma-Aldrich Co. and used without further purification. Pyridine, THF, toluene, and

benzene were dried and purified according to the known techniques and then used as solvents. Tris(4-bromo-2-methoxyphenyl)amine was obtained as described in ref. 40. All reactions, unless stated otherwise, were carried out under an inert atmosphere.

4.3. Synthesis of the oligomers

2,2′-Bithiophene-5-carbaldehyde (1a). 1.6 M solution of butyl lithium (13.27 mL, 21.2 mmol) in hexane was added dropwise to a solution of 2,2′-bithiophene (7.98 g, 48.0 mmol) in 220 mL of dry THF at −78 °C. Afterwards the reaction mixture was stirred for 60 min at −78 °C and then anhydrous DMF (5.26 mL, 72.0 mmol) was added in one portion. The reaction mixture was stirred for 1 h at −78 °C, then the cooling bath was removed, and the stirring was continued for 1 h. After completion of the reaction, 50 mL of 1 M HCl were added to the reaction mixture followed by the addition of 300 mL of freshly distilled diethyl ether and 150 mL of distilled water. The organic phase was separated, washed with water, and dried over sodium sulfate and filtered to give the product (8.8 g, 94%) as a red solid. M.p.: 55–56 °C. The product was used in the subsequent synthesis without further purification. ^{1}H NMR (250 MHz, $CDCl_3$, δ, ppm): 7.05 (dd, 1H, J_1 = 4.0 Hz, J_2 = 4.0 Hz), 7.23 (d, 1H, J = 4.0 Hz), 7.34 (d, 2H, J = 4.3 Hz), 7.65 (d, 1H, J = 4.0 Hz), 9.85 (s, 1H). ^{13}C NMR (125 MHz, $CDCl_3$): δ [ppm] 124.26, 126.17, 127.12, 128.38, 136.03, 137.38, 141.68, 147.18, 182.59. Calcd (%) for $C_9H_6OS_2$: C, 55.64; H, 3.11; S, 33.01. Found: C, 55.79; H, 3.24; S, 32.97. MALDI MS: found m/z 194.27; calculated for $[M]^+$ 194.21.

1-(2,2′-Bithien-5-yl)propan-1-one (1b). $SnCl_4$ (33.43 g, 128.3 mmol) was added to a mixture of 2,2′-bithiophene (19.85 g, 119.4 mmol) and propionyl chloride (11.05 g, 119.4 mmol) in toluene (120 mL) at 0 °C. After stirring at 0 °C for about 2 h, ice was added and the reaction mixture was diluted with CH_2Cl_2. The mixture was washed successively with water and a saturated aqueous solution of $NaHCO_3$, then dried over Na_2SO_4. The solvent was evaporated under vacuum, and the crude product was purified by recrystallization from hexane affording **1b** as a white solid (26.2 g, 86% yield). M.p.: 96 °C. ^{1}H NMR (250 MHz, $CDCl_3$, d, ppm): 1.23 (t, 3H, J = 7.3 Hz), 2.90 (m, 2H, M = 4, J = 7.3 Hz), 7.05 (dd, 1H, J_1 = 3.7, J_2 = 1.1 Hz), 7.15 (d, 1H, J = 4.3 Hz), 7.28–7.33 (overlapping peaks, 2H), 7.58 (d, 1H, J = 4.3 Hz). ^{13}C NMR (75 MHz, $CDCl_3$): δ [ppm] 8.59, 32.16, 124.04, 125.46, 126.30, 128.16, 132.34, 136.38, 141.98, 145.11, 193.49. Calcd (%) for $C_{11}H_{10}OS_2$: C, 59.43; H, 4.53; S, 28.84. Found: C, 59.25; H, 4.44; S, 28.74. MALDI-MS: found m/z 222.43; calculated for $[M]^+$ 222.33.

1-(2,2′-Bithien-5-yl)heptan-1-one (1c). This compound was obtained by the method described above for compound **1b** using 2,2′-bithiophene (10 g, 60.1 mmol), $SnCl_4$ (16.83 g, 64.6 mmol), and heptanoyl chloride (8.94 g, 60.1 mmol). Purification of the crude product by column chromatography on silica gel (eluent hexane) gave compound **1c** (13.56 g, 80% yield) as a colorless liquid. ^{1}H NMR (250 MHz, $CDCl_3$, δ, ppm): 0.88 (t, 3H, J = 6.7 Hz), 1.27–1.42 (overlapping peaks, 6H), 1.73 (m, 2H, M = 5, J = 7.3 Hz), 2.85 (t, 2H, J = 7.3 Hz), 7.05 (dd, 1H, J_1 = 3.7 Hz, J_2 = 1.1 Hz), 7.15 (d, 1H, J = 4.3 Hz), 7.28–7.33 (overlapping peaks, 2H), 7.58 (d, 1H, J = 4.3 Hz). ^{13}C NMR (125 MHz, $CDCl_3$): δ [ppm] 14.03, 22.48, 24.85, 28.99, 31.58, 39.02, 124.06, 125.48, 126.33, 128.18, 132.48, 136.38, 142.32, 145.24, 193.27. Calcd (%) for $C_{15}H_{18}OS_2$: C, 64.71; H, 6.52; S, 23.03. Found: C, 64.87; H, 6.58; S, 22.97. MALDI-MS: found m/z 278.49; calculated for $[M]^+$ 278.44.

2-(2,2′-Bithien-5-yl)-5,5-dimethyl-1,3-dioxane (2a). 2,2-Dimethyl-1,3-propanediol (9.32 g, 89.6 mmol) and *p*-TosH (0.596 g, 3.1 mmol) were added to a solution of compound **1a** (8.7 g, 44.8 mmol) in dry benzene (90 mL). Afterwards, the mixture was stirred at reflux for 10 hours using a water separator. After that, the mixture was extracted with toluene and washed with distilled water. The combined organic phases were dried over sodium sulfate and filtered. The solvent was evaporated under vacuum and the residue was dried at 1 Torr. This crude product was purified by column chromatography on silica gel (eluent toluene) to give the pure product (12.15 g, 97%) as a white solid. M.p.: 61–62 °C. ^{1}H NMR (250 MHz, $CDCl_3$, δ, ppm): 0.79 (s, 3H), 1.28 (s, 3H), 3.61 (d, 2H, J = 11 Hz), 3.74 (d, 2H, J = 11 Hz), 5.61 (s, 1H), 6.98–7.05 (overlapping peaks, 3H), 7.14 (dd, 1H, J_1 = 1.0 Hz, J_2 = 3.7 Hz), 7.19 (dd, 1H, J_1 = 1.0 Hz, J_2 = 3.7 Hz). ^{13}C NMR (125 MHz, $CDCl_3$): δ [ppm] 21.84, 22.99, 30.23, 77.54, 98.17, 123.12, 123.87, 124.53, 125.70, 127.79, 137.34, 137.72, 140.19. Calcd (%) for $C_{14}H_{16}O_2S_2$: C, 59.97; H, 5.75; S, 22.87. Found: C, 60.11; H, 5.67; S, 22.80. MALDI MS: found m/z 280.15; calculated for $[M]^+$ 280.41.

5,5-Dimethyl-2-[5′-(4,4,5,5-tetramethyl-1,3,2-dioxaborolan-2-yl)-2,2′-bithien-5-yl]-1,3-dioxane (3a). 2.5 M solution of *n*-butyl lithium (15.59 mL, 39.0 mmol) in hexane was added dropwise to a solution of compound **2a** (10.93 g, 39.0 mmol) in 270 mL of dry THF at −78 °C. Afterwards the reaction mixture was stirred for 60 min at −78 °C and then isopropoxy-4,4,5,5-tetramethyl-1,3,2-dioxaborolane (7.3 mL, 39.0 mmol) was added in one portion. The reaction mixture was stirred for 1 h at −78 °C, then the cooling bath was removed, and the stirring was continued for 1 h. After completion of the reaction, 400 mL of freshly distilled diethyl ether, 150 mL of distilled water and 21.2 mL of 1 M HCl were added to the reaction mixture. The organic phase was separated, washed with water, and dried over sodium sulfate and filtered. The solvent was evaporated to give 15.68 g (99%) of the pure product as a gray solid. M.p.: 164–166 °C. The product was used in the subsequent synthesis without further purification. ^{1}H NMR (250 MHz, $CDCl_3$, δ, ppm): 0.79 (s, 3H), 1.27 (s, 3H), 1.33 (s, 12H), 3.61 (d, 2H, J = 11 Hz), 3.73 (d, 2H, J = 11 Hz), 5.60 (s, 1H), 7.01 (d, 1H, J = 3.7 Hz), 7.09 (d, 1H, J = 3.7 Hz), 7.20 (d, 1H, J = 3.7 Hz), 7.49 (d, 1H, J = 3.7 Hz). ^{13}C NMR (125 MHz, $CDCl_3$): δ [ppm] 21.83, 22.95, 24.75, 30.21, 77.51, 84.16, 98.09, 123.79, 125.07, 125.81, 137.54, 137.91, 140.81, 144.03. Calcd (%) for $C_{20}H_{27}BO_4S_2$: C, 59.11; H, 6.70; S, 15.78. Found: C, 59.25; H, 6.82; S, 15.70. MALDI-MS: found m/z 406.43; calculated for $[M]^+$ 406.37.

2-(2,2′-Bithien-5-yl)-2-ethyl-5,5-dimethyl-1,3-dioxane (2b). This compound was obtained by the method described for compound **2a** using **1b** (26.1 g, 117.3 mmol), 1,3-dimethyl-1,3-propanediol (73.36 g, 704.8 mmol) and *p*-TosH (1.56 g, 8.2 mmol). Purification by column chromatography on silica

gel (eluent: toluene : hexane : triethylamine 49.95 : 49.95 : 0.1) gave the pure compound **1b** (31.4 g, 81%) as a colorless liquid. ^{1}H NMR (250 MHz, $CDCl_3$, δ, ppm): 0.65 (s, 3H), 0.9 (t, 3H, J = 7.3 Hz), 1.22 (s, 3H), 1.84 (m, 2H, M = 4, J = 7.3 Hz), 3.69 (d, 2H, J = 11 Hz), 3.70 (d, 2H, J = 11 Hz), 6.85 (d, 1H, J = 3.7 Hz), 6.98 (dd, 1H, J_1 = 3.7 Hz, J_2 = 3.7 Hz), 7.05 (d, 1H, J = 3.7 Hz), 7.12–7.21 (overlapping peaks, 2H). ^{13}C NMR (75 MHz, $CDCl_3$): δ [ppm] 7.66, 21.96, 22.81, 29.88, 37.77, 71.92, 100.56, 123.33, 123.56, 124.32, 126.97, 127.80, 137.49, 137.64, 143.33. Calcd (%) for $C_{16}H_{20}O_2S_2$: C, 62.30; H, 6.54; S, 20.79. Found: C, 62.45; H, 6.65; S, 20.72. MALDI-MS: found m/z 308.56; calculated for $[M]^+$ 308.46.

2-Ethyl-5,5-dimethyl-2-[5′-(4,4,5,5-tetramethyl-1,3,2-dioxaborolan-2-yl)-2,2′-bithien-5-yl]-1,3-dioxane (3b). This compound was obtained by the method described for compound **3a** using **2b** (31.1 g, 101 mmol), 1.6 M solution of butyl lithium (62.01 mL, 101 mmol) in hexane, and IPTMDOB (18.76 g, 101 mmol) to give 41.5 g (95%) of the pure product (purity was 98% according to ^{1}H NMR) as a blue solid. M.p.: 119–120 °C. The product was used in the subsequent synthesis without further purification. ^{1}H NMR (250 MHz, $CDCl_3$, δ, ppm): 0.65 (s, 3H), 0.9 (t, 3H, J = 7.3 Hz), 1.22 (s, 3H), 1.34 (s, 12H), 1.84 (m, 2H, M = 4, J = 7.3 Hz), 3.39 (d, 2H, J = 11 Hz), 3.69 (d, 2H, J = 11 Hz), 6.85 (d, 1H, J = 3.7 Hz), 7.10 (d, 1H, J = 3.7 Hz), 7.19 (d, 1H, J = 3.7 Hz), 7.50 (d, 1H, J = 3.7 Hz). ^{13}C NMR (75 MHz, $CDCl_3$): δ [ppm] 7.67, 21.96, 22.80, 24.62, 24.81, 29.88, 37.78, 71.93, 84.22, 100.54, 124.06, 124.78, 127.12, 137.51, 137.98, 144.03, 144.19. Calcd (%) for $C_{22}H_{31}BO_4S_2$: C, 60.83; H, 7.19; S, 14.76. Found: C, 60.49; H, 7.25; S, 14.70. MALDI-MS: found m/z 434.27; calculated for $[M]^+$ 434.49.

2-Ethyl-5,5-dimethyl-2-(2,2′:5′,2″-terthien-5-yl)-1,3-dioxane (4b). In an inert atmosphere, degassed solutions of 2-bromothiophene (3.75 g, 23 mmol) and compound **3b** (8 g, 18 mmol) in a toluene/ethanol mixture (100/10 mL) and 2 M solution of aq. Na_2CO_3 (14 mL) were added to $Pd(PPh_3)_4$ (399 mg, 0.35 mmol). The reaction mixture was stirred under reflux for 20 h, then it was cooled to room temperature and poured into 100 mL of water and 100 mL of toluene. The organic phase was separated, washed with water, dried over sodium sulfate and filtered. The solvent was evaporated in vacuum and the residue was dried at 1 Torr. The product was purified by column chromatography on silica gel (eluent: toluene : triethylamine 99.9 : 0.1) to give the pure compound **4b** (5.39 g, 74%) as a yellow solid. M.p.: 93–94 °C. ^{1}H NMR (250 MHz, $CDCl_3$, δ, ppm): 0.66 (s, 3H), 0.92 (t, 3H, J = 7.3 Hz), 1.22 (s, 3H), 1.86 (m, 2H, M = 2, J = 7.3 Hz), 3.41 (d, 2H, J = 11 Hz), 3.71 (d, 2H, J = 11 Hz), 6.86 (d, 1H, J = 3.7 Hz), 6.98–7.08 (overlapping peaks, 4H), 7.15 (dd, 1H, J_1 = 1 Hz, J_2 = 1 Hz), 7.20 (dd, 1H, J_1 = 1 Hz, J_2 = 1 Hz). ^{13}C NMR (75 MHz, $CDCl_3$): δ [ppm] 7.65, 21.91, 22.75, 29.84, 37.72, 71.87, 100.49, 123.25, 123.65, 124.08, 124.30, 124.46, 127.06, 127.87, 136.13, 136.17, 137.10, 137.28, 143.39. Calcd (%) for $C_{20}H_{22}O_2S_3$: C, 61.50; H, 5.68; S, 24.63. Found: C, 61.31; H, 5.75; S, 24.42. MALDI-MS: found m/z 389.56; calculated for [M] + 390.59.

2-Ethyl-5,5-dimethyl-2-[5″-(4,4,5,5-tetramethyl-1,3,2-dioxaborolan-2-yl)-2,2′:5′,2″-terthien-5-yl]-1,3-dioxane (5b). This compound was obtained by the method described for compound **3a** using **4b** (5.39 g, 14 mmol), 2.5 M solution of n-butyl lithium (5.52 mL, 14 mmol) in hexane, and IPTMDOB (2.57 g, 14 mmol) to give 6.92 g (98%) of the pure product (purity was 98% according to ^{1}H NMR) as a blue liquid. The product was used in the subsequent synthesis without further purification. ^{1}H NMR (250 MHz, $CDCl_3$, δ, ppm): 0.65 (s, 3H), 0.91 (t, 3H, J = 7.3 Hz), 1.22 (s, 3H), 1.34 (s, 12H), 1.86 (dd, 2H, J_1 = 7.3 Hz, J_2 = 7.3 Hz), 3.40 (d, 2H, J = 11 Hz), 3.70 (d, 2H, J = 11 Hz), 6.86 (d, 1H, J = 3.7 Hz), 7.04 (t, 2H, J = 3.7 Hz), 7.12 (d, 1H, J = 3.7 Hz), 7.21 (d, 1H, J = 3.7 Hz), 7.51 (d, 1H, J = 3.7 Hz). ^{13}C NMR (75 MHz, $CDCl_3$): δ [ppm] 7.62, 21.92, 22.76, 24.75, 25.60, 29.85, 37.72, 71.90, 84.20, 100.50, 123.44, 124.23, 124.82, 125.00, 127.07, 135.99, 136.89, 137.20, 137.96, 143.68, 143.75. Calcd (%) for $C_{26}H_{33}BO_4S_3$: C, 60.46; H, 6.44; S, 18.62. Found: C, 60.18; H, 6.28; S, 18.09. MALDI-MS: found m/z 515.61; calculated for $[M]^+$ 516.55.

2-(2,2′-Bithien-5-yl)-2-hexyl-5,5-dimethyl-1,3-dioxane (2c). This compound was obtained by the method described above for compound **2a** using **1c** (16.7 g, 60.1 mmol), 1,3-dimethyl-1,3-propanediol (37.56 g, 360.7 mmol), and p-TosH (0.8 g, 4.2 mmol) to give the crude product. It was purified by column chromatography on silica gel (eluent: toluene : hexane : triethylamine 49.95 : 49.95 : 0.1) to give the pure compound (15.07 g, 71%) as a colorless liquid. ^{1}H NMR (250 MHz, $CDCl_3$, δ, ppm): 0.65 (s, 3H), 0.84 (t, 3H, J = 6.7 Hz), 1.21–1.46 (overlapping peaks, 12H), 1.82–1.89 (overlapping peaks, 2H), 3.39 (d, 2H, J = 11 Hz), 3.71 (d, 2H, J = 11 Hz), 6.85 (d, 1H, J = 3.7 Hz), 6.97–7.02 (dd, 1H, J_1 = 3.7 Hz, J_2 = 3.7 Hz), 7.05 (d, 1H, J = 3.7 Hz), 7.12–7.17 (dd, 1H, J_1 = 1 Hz, J_2 = 1 Hz), 7.17–7.23 (dd, 1H, J_1 = 1 Hz, J_2 = 1 Hz). ^{13}C NMR (75 MHz, $CDCl_3$): δ [ppm] 14.05, 21.89, 22.59, 22.80, 23.11, 29.29, 29.80, 31.79, 44.98, 71.84, 100.29, 123.27, 123.49, 124.26, 126.78, 127.75, 137.43, 137.51, 143.62. Calcd (%) for $C_{20}H_{28}O_2S_2$: C, 65.89; H, 7.74; S, 17.59. Found: C, 65.45; H, 7.95; S, 17.32. MALDI-MS: found m/z 364.83; calculated for $[M]^+$ 364.56.

2-Hexyl-5,5-dimethyl-2-[5′-(4,4,5,5-tetramethyl-1,3,2-dioxaborolan-2-yl)-2,2′-bithien-5-yl]-1,3-dioxane (3c). This compound was obtained by the method described above for compound **3a** using **2c** (7.94 g, 22 mmol), 2.5 M solution of butyl lithium (8.71 mL, 22 mmol) in hexane, and IPTMDOB (4.05 g, 22 mmol) to give 9.91 g (92%) of the pure product (purity was 98% according to ^{1}H NMR) as a blue liquid. The product was used in the subsequent synthesis without further purification. ^{1}H NMR (250 MHz, $CDCl_3$, δ, ppm): 0.64 (s, 3H), 0.81 (t, 3H, J = 6.7 Hz), 1.22 (s, 12H), 1.33–1.46 (overlapping peaks, 12H), 1.82–1.86 (overlapping peaks, 2H), 3.38 (d, 2H, J = 11 Hz), 3.69 (d, 2H, J = 11 Hz), 6.85 (d, 1H, J = 3.7 Hz), 7.10 (d, 1H, J = 3.7 Hz), 7.19 (d, 1H, J = 3.7 Hz), 7.49 (d, 1H, J = 3.7 Hz). ^{13}C NMR (75 MHz, $CDCl_3$): δ [ppm] 14.04, 21.88, 22,58, 22.78, 23.09, 24.73, 29.27, 29.80, 31.78, 44.97, 71.84, 84.14, 100.26, 124.00, 127.70, 126.91, 137.39, 137.90, 144.13, 144.36. Calcd (%) for $C_{26}H_{39}BO_4S_2$: C, 63.66; H, 8.01; S, 13.07. Found: C, 63.18; H, 8.48; S, 12.89. MALDI-MS: found m/z 490.96; calculated for $[M]^+$ 490.54.

2-Hexyl-5,5-dimethyl-2-(2,2′:5′,2″-terthien-5-yl)-1,3-dioxane (4c). 2-Hexyl-5,5-dimethyl-2-(2,2′:5′,2″-terthien-5-yl)-1,3-dioxane (**4c**) was obtained by the method described above for compound **4b** using **3c** (8.7 g, 18 mmol), 2-bromothiopene (3.62 g, 22 mmol), 2 M solution of aq. Na_2CO_3 (14 mL), and $Pd(PPh_3)_4$

(384 mg, 0.33 mmol) to give a crude product. It was purified by column chromatography on silica gel (eluent: toluene : hexane : triethylamine 49.95 : 49.95 : 0.1) to give the pure compound **4c** (5.56 g, 71%) as a yellow solid. M.p. 78–80 °C. ^{1}H NMR (250 MHz, $CDCl_3$, δ, ppm): 0.65 (s, 3H), 0.84 (t, 3H, J = 6.7 Hz), 1.22–1.46 (overlapping peaks, 12H), 1.82–1.89 (overlapping peaks, 2H), 3.40 (d, 2H, J = 11 Hz), 3.70 (d, 2H, J = 11 Hz), 6.85 (d, 1H, J = 3.7 Hz), 7.00–7.07 (overlapping peaks, 4H), 7.16 (dd, 1H, J_1 = 1 Hz, J_2 = 1 Hz), 7.20 (dd, 1H, J_1 = 1 Hz, J_2 = 1 Hz). ^{13}C NMR (75 MHz, $CDCl_3$): δ [ppm] 14.10, 21.92, 22.63, 22.81, 23.15, 29.32, 29.85, 31.82, 45.00, 77.44, 100.31, 123.28, 123.66, 124.09, 124.31, 124.47, 126.92, 127.88, 136.14, 136.21, 137.13, 137.24, 143.81. Calcd (%) for $C_{24}H_{30}O_2S_3$: C, 64.53; H, 6.77; S, 21.53. Found: C, 64.87; H, 6.63; S, 21.12. MALDI-MS: found m/z 447.07; calculated for $[M]^+$ 446.70.

2-Hexyl-5,5-dimethyl-2-[5″-(4,4,5,5-tetramethyl-1,3,2-dioxaborolan-2-yl)-2,2′:5′,2″-terthien-5-yl]-1,3-dioxane (5c). 2-Hexyl-5,5-dimethyl-2-[5″-(4,4,5,5-tetramethyl-1,3,2-dioxaborolan-2-yl)-2,2′:5′,2″-terthien-5-yl]-1,3-dioxane (**5c**) was obtained by the method described above for compound **5b** using **4c** (4.33 g, 10 mmol), 2.5 M solution of n-butyl lithium (3.87 mL, 10 mmol) in hexane, and IPTMDOB (1.8 g, 10 mmol) to give 5.45 g (98%) of the pure product (purity was 98% according to ^{1}H NMR) as a dark green liquid. The product was used in the subsequent synthesis without further purification. ^{1}H NMR (250 MHz, $CDCl_3$, δ, ppm): 0.65 (s, 3H), 0.81 (t, 3H, J = 6.7 Hz), 1.22 (s, 12H), 1.33–1.46 (overlapping peaks, 12H), 1.82–1.87 (overlapping peaks, 2H), 3.39 (d, 2H, J = 11 Hz), 3.69 (d, 2H, J = 11 Hz), 6.85 (d, 1H, J = 3.7 Hz), 7.03–7.07 (overlapping peaks, 2H), 7.12 (d, 1H, J = 3.7 Hz), 7.21 (d, 1H, J = 3.7 Hz), 7.51 (d, 1H, J = 3.7 Hz). ^{13}C NMR (75 MHz, $CDCl_3$): δ [ppm] 14.04, 21.88, 22.78, 23.09, 24.75, 29.27, 29.80, 31.78, 44.98, 71.90, 84.20, 100.50, 123.44, 124.23, 124.82, 125.00, 127.07, 135.99, 136.89, 137.20, 137.96, 143.68, 143.75. Calcd (%) for $C_{30}H_{41}BO_4S_3$: C, 62.92; H, 7.22; S, 16.80. Found: C, 63.38; H, 7.54; S, 16.97. MALDI-MS: found m/z 572.67; calculated for $[M]^+$ 572.66.

Tris{4-[5′-(5,5-dimethyl-1,3-dioxan-2-yl)-2,2′-bithien-5-yl]-2-methoxyphenyl}amine (6a). In an inert atmosphere, degassed solutions of tris(4-bromo-2-methoxyphenyl) amine (2.5 g, 4.37 mmol) and compound **3a** (6.39 g, 15.7 mmol) in a toluene/ethanol mixture (110/11 mL) and 2 M solution of aq. Na_2CO_3 (23.6 mL) were added to $Pd(PPh_3)_4$ (545 mg, 0.47 mmol). The reaction mixture was stirred under reflux for 11 h, then it was cooled to room temperature and poured into 100 mL of water and 100 mL of toluene. The organic phase was separated, washed with water, dried over sodium sulfate and filtered. The solvent was evaporated under vacuum and the residue was dried at 1 Torr. The product was purified by column chromatography on silica gel (eluent: toluene : ethyl acetate : trimethylamine = 20 : 1 : 0.02) to give the pure compound **6a** (4.25 g, 83%) as a yellow solid. M.p. = 239–241 °C. ^{1}H NMR (250 MHz, $CDCl_3$): δ [ppm] 0.8 (s, 9H), 1.29 (s, 9H), 3.62 (d, 6H, J = 11 Hz), 3.65 (s, 9H), 3.74 (d, 6H, J = 11 Hz), 5.61 (s, 3H), 6.77–6.92 (overlapping peaks, 3H), 7.02–7.09 (overlapping peaks, 12H), 7.10 (d, 3H, J = 3.7 Hz), 7.12–7.20 (overlapping peaks, 3H). Calcd (%) for $C_{63}H_{63}NO_9S_6$: C, 64.64; H, 5.42; N, 1.20; S, 14.43. Found: C, 64.87; H, 5.63; N, 1.17; S, 14.32. MALDI-MS: found m/z 1169.47; calculated for $[M]^+$ 1170.57.

5′,5″,5‴-[Nitrilotris(3-methoxy-4,1-phenylene)]tris(2,2′-bithiophene-5-carbaldehyde) (7a). 1 M HCl (9 mL) was added to a solution of compound **6a** (3.4 g, 2.9 mmol) in THF (90 mL) and then the reaction mixture was stirred for 4 hours at reflux. During the reaction, the product was gradually formed as an orange precipitate. The organic phase was separated using diethyl ether, washed with water and filtered off. After completion of the reaction the organic phase was separated using diethyl ether, washed with water and filtered off to give the pure compound **7a** (2.5 g, 95%) as orange crystals. M.p. = 194–196 °C. ^{1}H NMR (250 MHz, DMSO-d_6): δ [ppm] 3.62 (s, 9H), 6.67 (d, 3H, J = 8.3 Hz), 7.16 (dd, 3H, J_1 = 1.82 Hz, J_2 = 1.82 Hz), 7.30 (d, 3H, J = 2.14 Hz), 7.53 (d, 6H, J = 3.7 Hz), 7.61 (dd, 3H, J_1 = 3.7 Hz, J_2 = 3.7 Hz), 7.98 (d, 3H, J = 3.7 Hz), 9.87 (s, 3H). Calcd (%) for $C_{48}H_{33}NO_6S_6$: C, 63.20; H, 3.65; N, 1.54; S, 21.09. Found: C, 63.31; H, 3.56; N, 1.58; S, 21.18. MALDI-MS: found m/z 911.75; calculated for $[M]^+$ 912.17.

Tris{4-[5′-(1,1-dicyanoeth-1-en-2-yl)-2,2′-bithien-5-yl]-2-methoxyphenyl}amine N(Ph-OMe-2T-DCV)$_3$. Compound **7a** (0.738 g, 0.8 mmol), malononitrile (0.32 g, 4.9 mmol) and dry pyridine (14.7 mL) were placed in a reaction vessel and stirred under an argon atmosphere for 6 hours at 105 °C using the microwave heating. After completion of the reaction, pyridine was evaporated under vacuum and the residue was dried at 1 Torr. This crude product was purified by column chromatography on silica gel (eluent: dichloromethane). Further purification included precipitation of the product from its THF solution with toluene and hexane to give the pure product as a black solid (0.43 g, 51%). M.p. = 200 °C. ^{1}H NMR (250 MHz, DMSO-d6): δ [ppm] 3.62 (s, 9H), 6.75 (d, 3H, J = 8.6 Hz), 7.18–7.24 (overlapping peaks, 3H), 7.29–7.34 (overlapping peaks, 3H), 7.61 (t, 6H, J = 3.7 Hz), 7.70 (d, 3H, J = 3.7 Hz), 7.88 (d, 3H, J = 4.3 Hz), 8.61 (s, 3H). Calcd (%) for $C_{57}H_{33}N_7O_3S_6$: C, 64.81; H, 3.15; N, 9.28; S, 18.21. Found: C, 64.72; H, 3.16; N, 9.22; S, 18.18. MALDI-MS: found m/z 1056.26; calculated for $[M]^+$ 1056.21.

Tris{4-[5″-(2-ethyl-5,5-dimethyl-1,3-dioxan-2-yl)-2,2′:5′,2″-terthien-5-yl]-2-methoxyphenyl}amine (6b). This compound was obtained by the method described for compound **6a** using tris(4-bromo-2-methoxyphenyl)amine (1.71 g, 2.99 mmol), compound **5b** (5.56 g, 10.8 mmol), 2 M solution of aq. Na_2CO_3 (16.1 mL), and $Pd(PPh_3)_4$ (0.37 g, 0.32 mmol). The crude product was purified by column chromatography on silica gel (eluent: toluene : triethylamine = 1000 : 1) to give the pure compound **6b** (4.06 g, 89%) as a yellow solid. M.p. = 185–187 °C. ^{1}H NMR (250 MHz, $CDCl_3$): δ [ppm] 0.67 (s, 9H), 0.93 (t, 9H, J = 7.3 Hz), 1.24 (s, 9H), 1.87 (dd, 6H, J_1 = 7.3 Hz, J_2 = 7.3 Hz), 3.41 (d, 6H, J = 11 Hz), 3.67 (s, 9H), 3.72 (d, 6H, J = 11 Hz), 6.81–6.98 (overlapping peaks, 6H), 7.02–7.21 (overlapping peaks, 21H). Calcd (%) for $C_{81}H_{81}NO_9S_9$: C, 64.81; H, 5.44; N, 0.93; S, 19.22. Found: C, 64.57; H, 5.63; N, 0.95; S, 19.11. MALDI-MS: found m/z 1501.82; calculated for $[M]^+$ 1501.12.

1,1′,1″-{Nitrilotris[(3-methoxy-4,1-phenylene)-2,2′:5′,2″-terthiene-5″,5-diyl]}tripropan-1-one (7b). This compound was obtained by the method described for compound **7a** using 1 M HCl (4.5 mL), **6b** (3.35 g, 2.23 mmol) and THF (67 mL) to yield the pure compound **7b** (2.48 g, 91%) as orange crystals. M.p. = 256–257 °C. ^{1}H NMR (250 MHz, $CDCl_3$): δ [ppm] 1.21 (t, 9H, J = 7 Hz),

2.84–3.00 (m, 6H, M = 4, J = 7.3 Hz), 3.67 (s, 9H), 6.85 (d, 3H, J = 8.5 Hz), 7.04–7.24 (overlapped peaks, 21H), 7.59 (d, 3H, J = 4 Hz). Calcd (%) for $C_{66}H_{51}NO_6S_9$: C, 63.79; H, 4.14; N, 1.13; S, 23.22. Found: C, 63.31; H, 4.26; N, 1.22; S, 23.58. MALDI-MS: found m/z 1241.16; calculated for $[M]^+$ 1242.72.

Tris{4-[5″-(1,1-dicyanobut-1-en-2-yl)-2,2′:5′,2″-terthien-5-yl]-2-methoxyphenyl}amine N(Ph-OMe-3T-DCV-Et)$_3$. This compound was obtained by the method described for N(Ph-OMe-2T-DCV)$_3$ using compound **7b** (2.11 g, 1.7 mmol) and malononitrile (0.56 g, 8.5 mmol) to give the pure product as a black solid (0.4 g, 18%). M.p. = 243 °C. ^{1}H NMR (250 MHz, $CDCl_3$): δ [ppm] 1.34 (t, 9H, J = 7.3 Hz), 2.92 (m, 6H, M = 4, J = 7 Hz), 3.68 (s, 9H), 6.86 (d, 3H, J = 8.6 Hz), 7.04–7.13 (overlapping peaks, 6H), 7.14 (d, 3H, J = 3.7 Hz), 7.18–7.23 (overlapping peaks, 6H), 7.26–7.28 (overlapping peaks, 3H), 7.29 (d, 3H, J = 3.7 Hz), 7.96 (d, 3H, J = 3.7 Hz). Calcd (%) for $C_{75}H_{51}N_7O_3S_9$: C, 64.95; H, 3.71; N, 7.07; S, 20.81. Found: C, 64.34; H, 3.92; N, 6.85; S, 20.37. MALDI-MS: found m/z 1385.62; calculated for $[M]^+$ 1386.86.

Tris{4-[5″-(2-ethyl-5,5-dimethyl-1,3-dioxan-2-yl)-2,2′:5′,2″-terthien-5-yl]-2-methoxyphenyl}amine (6c). This compound was obtained by the method described above for compound **6a** using tris-(4-bromo-2-methoxyphenyl)amine (1.00 g, 1.75 mmol), compound **5c** (3.6 g, 6.29 mmol), 2 M solution of aq. Na_2CO_3 (9.4 mL), and $Pd(PPh_3)_4$ (218 mg, 0.19 mmol). The crude product was purified by column chromatography on silica gel (eluent: toluene : triethylamine = 1000 : 1) to give the pure compound **6c** (2.04 g, 70%) as a yellow solid. M.p. = 92–93 °C. ^{1}H NMR (250 MHz, $CDCl_3$): δ [ppm] 0.66 (s, 9H), 0.82 (t, 9H, J = 6.7 Hz), 1.19–1.48 (overlapped peaks, 33H), 1.72–2.01 (overlapped peaks, 6H), 3.40 (d, 6H, J = 11 Hz), 3.67 (s, 9H), 3.70 (d, 6H, J = 11 Hz), 6.87 (d, 6H, J = 3.7 Hz), 7.04–7.20 (overlapped peaks, 21H). Calcd (%) for $C_{93}H_{105}NO_9S_9$: C, 66.91; H, 6.34; N, 0.84; S, 17.29. Found: C, 66.87; H, 6.53; N, 0.89; S, 17.12. MALDI-MS: found m/z 1669.32; calculated for $[M]^+$ 1669.41.

1,1′,1″-{Nitrilotris[(3-methoxy-4,1-phenylene)-2,2′:5′,2″-terthiene-5″,5-diyl]}triheptan-1-one (7c). Compound **7c** was obtained by the method described above for compound **7b** using 1 M HCl (2.7 mL), compound **6c** (1.52 g, 0.91 mmol) and THF (35 mL) to give pure compound **7c** (1.17 g, 91%) as orange crystals. M.p. = 245–247 °C. ^{1}H NMR (250 MHz, $CDCl_3$): δ [ppm] 0.85 (t, 9H, J = 6.7 Hz), 1.22–1.47 (overlapped peaks, 24H), 2.00 (t, 6H, J = 7.3 Hz), 3.67 (s, 9H), 6.89 (d, 3H, J = 3.7 Hz), 6.98–7.09 (overlapped peaks, 9H), 7.11–7.18 (overlapped peaks, 12H), 7.48 (d, 3H, J = 4.1 Hz). Calcd (%) for $C_{78}H_{75}NO_6S_9$: C, 66.40; H, 5.36; N, 0.99; S, 20.45. Found: C, 66.48; H, 5.49; N, 1.08; S, 21.01. MALDI-MS: found m/z 1411.07; calculated for $[M]^+$ 1411.05.

Tris{4-[5″-(1,1-dicyanooct-1-en-2-yl)-2,2′:5′,2″-terthien-5-yl]-2-methoxyphenyl}amine N(Ph-OMe-3T-DCV-Hex)$_3$. This compound was obtained by the method described above for N(Ph-OMe-2T-DCV)$_3$ using compound **8c** (1 g, 0.7 mmol), malononitrile (0.327 g, 5.0 mmol) and pyridine (20 mL) to give the pure product as a black solid (0.77 g, 70%). M.p. = 173 °C. ^{1}H NMR (250 MHz, $CDCl_3$): δ [ppm] 0.87 (t, 9H, J = 6.7 Hz), 1.29–1.51 (overlapping peaks, 18H), 1.63–1.76 (overlapping peaks, 6H), 2.88 (t, 6H, J = 7.3 Hz), 3.68 (s, 9H), 6.86 (d, 3H, J = 8.6 Hz), 7.06–7.25 (overlapping peaks, 18H), 7.29 (d, 3H, J = 3.7 Hz), 7.94 (d, 3H, J = 4.3 Hz). Calcd (%) for $C_{87}H_{75}N_7O_3S_9$: C, 67.19; H, 4.86; N, 6.30; S, 18.56. Found: C, 67.09; H, 4.93; N, 6.22; S, 18.31. MALDI-MS: found m/z 1555.53; calculated for $[M]^+$ 1555.19.

Acknowledgements

A part of this work including the synthesis and characterization of the oligomers was carried out under financial support from the Russian Science Foundation (grant 14-13-01380). The preparation and characterization of blends and the photovoltaic devices were financed by the Cluster of Excellence ''Engineering of Advanced Materials'' at the University of Erlangen-Nuremberg, which was funded by the German Research Foundation (DFG) within the framework of its ''Excellence Initiative''. This work was partially funded by the Sonderforschungsbereich 953 ''Synthetic Carbon Allotropes'', and we also thank the support of the ''Solar Technologies go Hybrid'' (SolTech) project and the Energy Campus Nürnberg (EnCN) financed by the Bavarian state government.

References

1 C. Brabec, U. Scherf and V. Dyakonov, *Organic Photovoltaics Materials, Device Physics, and Manufacturing Technologies*, Willey, 2nd edn, 2014.
2 W. Cao and J. Xue, *Energy Environ. Sci.*, 2014, **7**, 2123.
3 J. Yu, Y. Zheng and J. Huang, *Polymers*, 2014, **6**, 2473.
4 R. S. Kularatne, H. D. Magurudeniya, P. Sista, M. C. Biewer and M. C. Stefan, *J. Polym. Sci., Part A: Polym. Chem.*, 2013, **51**, 743.
5 A. Mishra and P. Bauerle, *Angew. Chem., Int. Ed.*, 2012, **51**, 2020.
6 J. Roncali, P. Leriche and P. Blanchard, *Adv. Mater.*, 2014, **26**, 3821.
7 W. Ni, X. Wan, M. Li, Y. Wang and Y. Chen, *Chem. Commun.*, 2015, **51**, 4936.
8 Q. Zhang, B. Kan, F. Liu, G. Long, X. Wan, X. Chen, Y. Zuo, W. Ni, H. Zhang, M. Li, Z. Hu, F. Huang, Y. Cao, Z. Liang, M. Zhang, T. P. Russell and Y. Chen, *Nat. Photonics*, 2015, **9**, 35.
9 K. Sun, Z. Xiao, S. Lu, W. Zajaczkowski, W. Pisula, E. Hanssen, J. M. White, R. M. Williamson, J. Subbiah, J. Ouyang, A. B. Holmes, W. W. H. Wong and D. J. Jones, *Nat. Commun.*, 2015, **6**, 6013.
10 A. Mishra, C.-Q. Ma and P. Bäuerle, *Chem. Rev.*, 2009, **109**, 1141.
11 K. Schulze, C. Uhrich, R. Schüppel, K. Leo, M. Pfeiffer, E. Brier, E. Reinold and P. Bäuerle, *Adv. Mater.*, 2006, **18**, 2872.
12 S. Roquet, A. Cravino, P. Leriche, O. Alévêque, P. Frère and J. Roncali, *J. Am. Chem. Soc.*, 2006, **128**, 3459.
13 S. Mannam and G. Sekar, *Tetrahedron Lett.*, 2008, **49**, 1083.
14 F. Silvestri, M. Jordan, K. Howes, M. Kivala, P. Rivera-Fuentes, C. Boudon, J.-P. Gisselbrecht, W. B. Schweizer, P. Seiler, M. Chiu and F. Diederich, *Chem. – Eur. J.*, 2011, **17**, 6088.

15 J. Min, Y. N. Luponosov, T. Ameri, A. Elschner, S. M. Peregudova, D. Baran, T. Heumüller, N. Li, F. Machui, S. Ponomarenko and C. J. Brabec, *Org. Electron.*, 2013, **14**, 219.
16 S. Ponomarenko, Y. N. Luponosov, J. Min, A. N. Solodukhin, N. Surin, M. Shcherbina, S. N. Chvalun, T. Ameri and C. J. Brabec, *Faraday Discuss.*, 2014, **174**, 313.
17 J. Min, Y. N. Luponosov, A. Gerl, M. S. Polinskaya, S. M. Peregudova, P. V. Dmitryakov, A. V. Bakirov, M. A. Shcherbina, S. N. Chvalun, S. Grigorian, N. Kausch-Busies, S. A. Ponomarenko, T. Ameri and C. J. Brabec, *Adv. Energy Mater.*, 2014, **4**, 1301234.
18 Y. N. Luponosov, J. Min, A. N. Solodukhin, S. N. Chvalun, T. Ameri, C. J. Brabec and S. A. Ponomarenko, *Proc. SPIE*, 2015, **9567**, 95670W, DOI: 10.1117/12.2187454.
19 J. Zhou, X. Wan, Y. Liu, G. Long, F. Wang, Z. Li, Y. Zuo, C. Li and Y. Chen, *Chem. Mater.*, 2011, **23**, 4666.
20 J. Min, Y. N. Luponosov, N. Gasparini, M. Richter, A. V. Bakirov, M. A. Shcherbina, S. N. Chvalun, L. Grodd, S. Grigorian, T. Ameri, S. A. Ponomarenko and C. J. Brabec, *Adv. Energy Mater.*, 2015, **5**, 1500386.
21 A. K. K. Kyaw, D. H. Wang, V. Gupta, J. Zhang, S. Chand, G. C. Bazan and A. J. Heeger, *Adv. Mater.*, 2013, **25**, 2397.
22 W. Li, W. Deng, K. Wu, G. Xie, C. Yang, H. Wu and Y. Cao, *J. Mater. Chem. C*, 2016, **4**, 1978.
23 Y. Liu, X. Wan, F. Wang, J. Zhou, G. Long, J. Tian and Y. Chen, *Adv. Mater.*, 2011, **23**, 5387.
24 C. V. Kumar, L. Cabau, E. N. Koukaras, G. D. Sharma and E. Palomares, *Org. Electron.*, 2015, **26**, 36.
25 C. D. Wessendorf, G. L. Schulz, A. Mishra, P. Kar, I. Ata, M. Weidelener, M. Urdanpilleta, J. Hanisch, E. Mena-Osteritz, M. Lindén, E. Ahlswede and P. Bäuerle, *Chem. Commun.*, 2013, **49**, 10865.
26 H. Shang, H. Fan, Y. Liu, W. Hu, Y. Li and X. Zhan, *Adv. Mater.*, 2011, **23**, 1554.
27 Yu. N. Luponosov, A. N. Solodukhin and S. A. Ponomarenko, *Polym. Sci., Ser. C*, 2014, **56**, 104.
28 S. Paek, N. Cho, S. Cho, J. K. Lee and J. Ko, *Org. Lett.*, 2012, **14**, 6326.
29 J. Kwak, Y.-Y. Lyu, H. Lee, B. Choi, K. Char and C. Lee, *J. Mater. Chem.*, 2012, **22**, 6351.
30 Z. Jiang, T. Ye, C. Yang, D. Yang, M. Zhu, C. Zhong, J. Qin and D. Ma, *Chem. Mater.*, 2011, **23**, 771.
31 S. Paek, H. Choi, J. Sim, K. Song, J. K. Lee and J. Ko, *J. Phys. Chem. C*, 2014, **118**, 27193.
32 D. Demeter, V. Jeux, P. Leriche, P. Blanchard, Y. Olivier, J. Cornil, R. Po and J. Roncali, *Adv. Funct. Mater.*, 2013, **23**, 4854.
33 S. Maniam, A. B. Holmes, G. A. Leeke, A. Bilic and G. E. Collis, *Org. Lett.*, 2015, **17**, 4022.
34 J. Min, Y. N. Luponosov, A. N. Solodukhin, N. Kausch-Busies, S. A. Ponomarenko, T. Ameri and C. J. Brabec, *J. Mater. Chem. C*, 2014, **2**, 7614.
35 J. Min, Y. N. Luponosov, D. Baran, S. N. Chvalun, M. A. Shcherbina, A. V. Bakirov, P. V. Dmitryakov, S. M. Peregudova, N. Kausch-Busies, S. A. Ponomarenko, T. Ameri and C. J. Brabec, *J. Mater. Chem. A*, 2014, **2**, 16135.
36 C. Soulie, P. Bassoul and J. Simon, *New J. Chem.*, 1993, **17**, 787.
37 O. V. Kozlov, Yu. N. Luponosov, S. A. Ponomarenko, N. Kausch-Busies, Yu. D. Paraschuk, Y. Olivier, D. Beljonne, J. Cornil and M. S. Pshenichnikov, *Adv. Energy Mater.*, 2015, **5**, 1401657.
38 (*a*) S. A. Ponomarenko, S. Kirchmeyer, A. Elschner, N. M. Alpatova, M. Halik, H. Klauk, U. Zschieschang and G. Schmid, *Chem. Mater.*, 2006, **18**, 579; (*b*) S. A. Ponomarenko, N. N. Rasulova, Y. N. Luponosov, N. M. Surin, M. I. Buzin, I. Leshchiner, S. M. Peregudova and A. M. Muzafarov, *Macromolecules*, 2012, **45**, 2014.
39 M. D. Perez, C. Borek, S. R. Forrest and M. E. Thompson, *J. Am. Chem. Soc.*, 2009, **131**, 9281.
40 R. Alvarez and G. H. Mehl, *Tetrahedron Lett.*, 2005, **46**, 67.

